

1 **Reframing gullies as recharge zones in dryland landscapes of the Loess Plateau, China**

2

3 Zhenxia Ji<sup>a,b,c,d</sup>, Alan D. Ziegler<sup>e</sup>, Li Wang<sup>a,b,c,d</sup>

4 <sup>a</sup> State Key Laboratory of Soil and Water Conservation and Desertification Control, College of Natural  
5 Resources and Environment, Northwest A&F University, Yangling 712100, China

6 <sup>b</sup> College of Soil and Water Conservation Science and Engineering, Northwest A&F University, Yangling  
7 712100, China

8 <sup>c</sup> State Key Laboratory of Soil and Water Conservation and Desertification Control, Chinese Academy of  
9 Sciences and the Ministry of Water Resources, Yangling 712100, China

10 <sup>d</sup> Institute of Soil and Water Conservation, Chinese Academy of Sciences and the Ministry of Water  
11 Resources, Yangling 712100, China

12 <sup>e</sup> Andaman Coastal Station for Research and Development, Kasetsart University, Ranong, Thailand

13

14 Correspondence to: Li Wang (wangli5208@nwsuaf.edu.cn)

15 State Key Laboratory of Soil and Water Conservation and Desertification Control, Institute of Soil and  
16 Water Conservation, Northwest A&F University.

17 Address: Xinong Road, #26, Yangling, Shaanxi Province 712100, China

18

删除了:

23 **Abstract**

24 Large gullies in dryland landscapes are often indicators of land degradation by surface runoff.  
25 However, under conditions where gully systems are hydrologically arrested by restoration interventions  
26 that increase water residence time—most notably check dams and ponds—they may also function as  
27 hydrologically active zones of groundwater recharge and subsurface connectivity. In China's Loess  
28 Plateau, we assess these functions in the Nianzhuang Catchment using a multi-indicator, process-based  
29 approach that integrates stable isotopes ( $\delta^2\text{H}$ ,  $\delta^{18}\text{O}$ ), chloride concentrations, and groundwater level  
30 fluctuations. Our results show that precipitation is the dominant source of recharge for shallow pore water  
31 within engineered gully zones, while deeper fissure water is replenished more slowly through percolation.  
32 Hydrological arrest through ecological engineering interventions acts as focal points for groundwater  
33 infiltration, enhancing recharge in otherwise limited dryland systems. Estimated annual recharge in the  
34 monitored gully-zone pore aquifer (238–241 mm) is equivalent to about 43% of the mean annual  
35 precipitation at the site, a site-specific recharge magnitude that far exceeds reported catchment-wide  
36 recharge rates observed in nearby tableland and hilly areas. Our results indicate that engineered gully  
37 systems can act as focused recharge zones rather than solely degraded landforms. By linking runoff  
38 convergence and ponding to measurable recharge responses, the study provides a process-based  
39 framework for assessing groundwater dynamics in managed semi-arid landscapes.

40

41 **Keywords:** surface water, spring water, pore water, fissure water, hydrological connectivity, groundwater  
42 recharge

43

44 **1. Introduction**

45 Groundwater recharge is a critical yet poorly understood component of hydrological cycles in  
46 dryland catchments (Ji et al., 2024a). It is shaped by the precipitation regime, surface landcover  
47 heterogeneity, integrity of the subsurface regolith, characteristics of the underlying bedrock, and human  
48 interventions (Vries and Simmers, 2002; Owuor et al., 2016; Salek et al., 2018; Xu and Beckman, 2019;  
49 Zhang et al., 2020; Li et al, 2024b; Medici et al., 2024). While favorable subsurface flow pathways can  
50 locally enhance recharge, dryland regions are highly sensitive to even slight changes in precipitation, soil  
51 moisture, or runoff generation. This heightened sensitivity reflects their position along climatic ecotones

删除了: viewed as

删除了:

删除了: However

删除了: However,, yet in some settings they may serve critical ecohydrological functions—supporting groundwater recharge and subsurface connectivity.

删除了: Restoration interventions—, particularly check dams and ponds—, act

删除了:

删除了: accounts for over

删除了: far exceeding

删除了: typical

带格式的: 行距: 1.5 倍行距

删除了: reference

删除了: the

删除了: the

67 and the influence of complex land–atmosphere–biosphere feedbacks (Kuang et al., 2019; Al-Oqaili et al.,  
68 2020; He et al., 2020; Jin et al., 2019; Jia et al., 2024). Small changes in these processes can cascade  
69 across catchments at various scales, amplifying existing vulnerabilities to ecological and social systems  
70 (Nicholson, 2011; Huang et al., 2017; Berg et al., 2016). In these fragile landscapes, understanding  
71 groundwater replenishment processes is crucial for sustaining ecosystems, securing water, and guiding  
72 restoration and management (Gleeson et al., 2016; Jasechko and Perrone, 2021; Scanlon et al., 2006).

73 Despite a growing body of research on groundwater recharge in (semi-) arid regions, significant  
74 knowledge gaps remain in landscapes with pronounced spatial heterogeneity, such as slopes, hilltops,  
75 and gully systems, where infiltration pathways and recharge processes can diverge sharply over short  
76 distances (Tooth, 2012; Manna et al., 2018; Letz et al., 2021). Gully systems, often seen as signs of land  
77 degradation, may beneficially act as recharge zones, capturing and infiltrating surface runoff during  
78 episodic rainfall (Tan et al., 2017; Li et al., 2024a; Xue et al., 2025). This same topographic focusing  
79 enables the rapid downslope transport of contaminants, including agricultural nutrients, sediments, and  
80 associated pollutants (Lian et al., 2025; Qu et al., 2025). However, the role of gullies in promoting vertical  
81 infiltration into groundwater is highly dependent on local subsurface connectivity and permeability  
82 conditions. Moreover, their broader hydrological functions remain poorly quantified, especially under  
83 the influence of widespread human interventions such as check dams and artificial ponds. While these  
84 structures are typically designed to arrest land surface degradation, they can substantially alter surface–  
85 subsurface connectivity and reshape recharge dynamics in uncertain ways (Lamontagne et al., 2021;  
86 Huang et al., 2019; Wang et al., 2023).

87 Worldwide, loess covers approximately 6% of the land surface area, forming discontinuous east–  
88 west belts in the mid-latitude forest-steppe, steppe, and desert-steppe zones of both hemispheres (Liu,  
89 1985; Pécsi, 1990; Li et al., 2020). Among these, the Chinese Loess Plateau, the focus of our study  
90 accounts for approximately 7.4% of the global loess area (635,280 km<sup>2</sup>; Li et al., 2020). It serves as a  
91 globally important natural laboratory for studying soil erosion and groundwater recharge processes, due  
92 to its exceptionally thick loess deposits (Li et al., 2021), highly erodible soils, intense summer rainstorms,  
93 and long history of agricultural activity, which collectively make it one of the most severely eroded  
94 regions worldwide (Shi and Shao, 2000; Fu et al., 2011). Its distinctive stratigraphic structure,  
95 characterized by thick, low-permeability loess layers, fundamentally governs groundwater behavior  
96 (Qiao et al., 2017). Meanwhile, extensive human interventions aimed at erosion control, including large-

删除了: Although favorable subsurface flow pathways can locally enhance recharge, dryland regions—situated along climatic ecotones and shaped by complex land–atmosphere–biosphere feedbacks—are highly sensitive to even modest shifts in water availability. Small changes in soil moisture or runoff routing can cascade across catchments at various scales, amplifying existing vulnerabilities to ecological and social systems (Nicholson, 2011; Huang et al., 2017; Berg et al., 2016).

删除了: —affected collectively by vegetation, geomorphology, and engineering—

删除了: key to

删除了: In these “fragile” and diverse landscapes, understanding the processes that govern when, where, and how groundwater is replenished—including the countervailing influences of vegetation dynamics, geomorphology, and engineered features—is essential for sustaining ecosystems, securing water resources, and informing land restoration and catchment management

删除了: —

删除了: gullies

删除了: —

删除了: paradoxically

删除了: Among these landforms, gully systems—often regarded as hallmarks of land degradation—may paradoxically serve as focal points for recharge, capturing and infiltrating surface runoff during episodic rainfall events

删除了: However, t

删除了: Notably, gully systems may facilitate the rapid downslope transport of contaminants such as agricultural nutrients and sediments

删除了: —

删除了: This study addresses these issues by focuses focusing on groundwater recharge in the gully systems in temperate loess soils.

删除了: ).

133 scale afforestation and gully engineering projects, have profoundly altered regional hydrological  
 134 processes and the spatial redistribution of water (Wang et al., 2020; Zhao et al., 2024).

135 The setting for our investigation is a semi-arid landscape that has been shaped by severe soil erosion,  
 136 extensively modified by engineered landforms; and it is now characterized by chronic water scarcity (Fu  
 137 et al., 1999; Liu et al., 2017; Liu and Li, 2017; Li et al., 2021; Huang et al., 2024). Water scarcity  
 138 manifests as declining groundwater levels, reduced streamflow, dried-up wells and springs, and limited  
 139 irrigation capacity (Yu et al., 2025). In such vulnerable environments, understanding the sources and  
 140 sustainability of groundwater recharge is critical for long-term water resource management (Ajjur and  
 141 Baalousha, 2021; Meles et al., 2024). Groundwater, for example, is a lifeline for rural communities in  
 142 the hilly–gully region, yet scientific attention has largely bypassed the gullies themselves. Most previous  
 143 studies have focused on recharge processes in tablelands and loess-covered hills, highlighting slow  
 144 “piston flow” as the dominant mechanism (Huang and Pang, 2011; Huang et al., 2013; Li et al., 2017;  
 145 Lu, 2020; Wang et al., 2024). However, the deep-profile recharge mechanisms observed in these areas  
 146 may not apply to the gully-dominated landscapes of the Loess Plateau (Wang et al., 2024; Qiao et al.,  
 147 2017; Zhu et al., 2018). Moreover, the hydrological functions of widely distributed gully systems,  
 148 especially under the influence of engineering structures such as check dams, remain insufficiently  
 149 quantified, and their underlying processes have long remained in the research shadow (Liu et al., 2011).

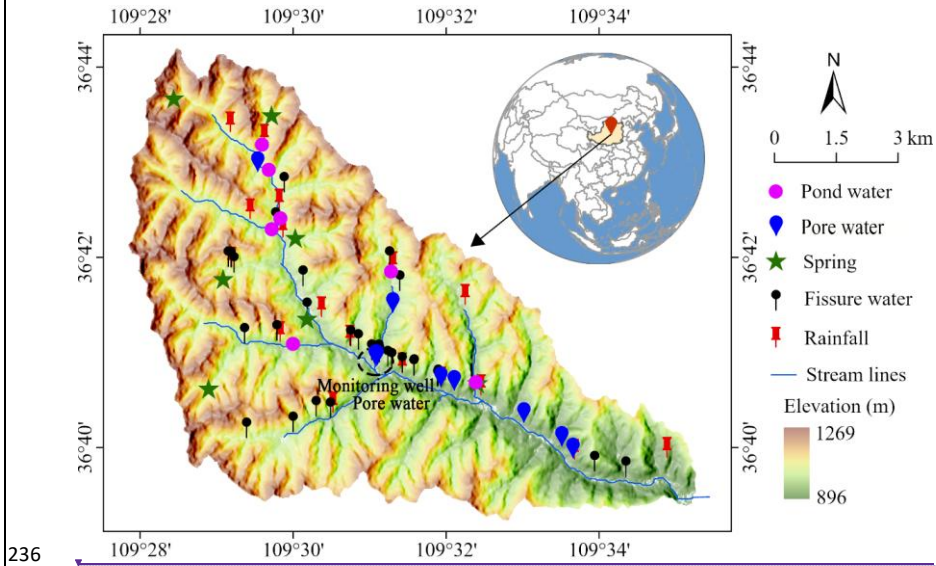
150 Therefore, this study selects the Nianzhuang Catchment, a typical gully area on the Loess Plateau  
 151 impacted by check dams, to establish a multi-method framework for assessing groundwater recharge by  
 152 integrating stable isotope analysis ( $\delta^2\text{H}$  and  $\delta^{18}\text{O}$ ), chloride concentrations, water table fluctuations, and  
 153 hydro-statistical modeling. Specifically, our goals are to: (1) characterize the isotopic and hydrochemical  
 154 signatures of precipitation, surface water (ponds), shallow pore water, and deeper fissure water; (2)  
 155 identify and trace hydraulic connections and flow paths of different water bodies; and (3) quantitatively  
 156 estimate pore-water recharge rates. This integrated approach aims to advance understanding of  
 157 groundwater dynamics in complex dryland terrains, reframes engineered gully systems as critical  
 158 recharge zones in engineered dryland landscapes, providing actionable insights for sustainable  
 159 groundwater management and ecological restoration in the Loess Plateau and similar semi-arid regions  
 160 worldwide.

161

- 删除了: ,
- 删除了: manifests
- 删除了: as
- 删除了: references
- 删除了:
- 删除了: Most prior research has centered on recharge processes in tablelands and loess-covered hills (Huang et al., 2011; Li et al., 2017; Lu, 2020; Wang et al., 2024), leaving the hydrological role of gully systems—despite their striking prominence in the landscape—largely in the shadows uncharted (Liu et al., 2011).
- 删除了: In this study, we
- 设置了格式: 字体: (默认) Times New Roman, (中文) Times New Roman
- 设置了格式: 字体: (默认) Times New Roman
- 删除了: integrate
- 删除了: to establish a multi-method framework for assessing groundwater recharge in gully systems of the Loess Plateau
- 删除了: we aim to
- 删除了: trace hydraulic connections, flow paths, and recharge mechanisms—distinguishing topographic-focused recharge in gullies from dispersed piston-flow recharge on hillslopes
- 设置了格式: 字体: (默认) Times New Roman
- 删除了: quantitatively estimate pore-water recharge rates while evaluating uncertainties and the amplifying role of restoration interventions (check dams and ponds)
- 删除了: By reconciling potential contradictions among methods and acknowledging risks such as enhanced pollutant transport, this complementary approach reframes gullies as critical recharge zones in engineered dryland landscapes, providing actionable insights for sustainable groundwater management and ecological restoration in the Loess Plateau and similar semi-arid regions worldwide. In this study, we integrate stable isotope analysis ( $\delta^2\text{H}$  and  $\delta^{18}\text{O}$ ), chloride concentration measurements, water table fluctuation estimations, and hydro-statistical modeling to de...
- 删除了: gullies
- 删除了: generating process-based insights critical for sustainable water and land management in gully-dominated...
- 删除了: ...

227 **2. Sampling site**

228 The Nianzhuang Catchment is located northwest of Yan'an City in Shaanxi Province, China  
229 (approximately 36°42'N, 109°31'E). As a tributary of the Yan River, which ultimately flows into the  
230 Yellow River, the catchment spans 53.94 km<sup>2</sup> and includes the well-studied Yangjuangou sub-catchment  
231 (3.11 km<sup>2</sup>; ~36°35'N, ~109°32'E), previously investigated in numerous hydrological and ecological  
232 studies (Fu et al., 1999; Fu et al., 2011; Fu et al., 2017; Liu and Li, 2017). Elevation ranges from 896 to  
233 1,269 m, with terrain gradually sloping from northwest to southeast (Fig. 1). The region experiences a  
234 semi-arid continental monsoon climate, with a mean annual precipitation of approximately 550 ± 100  
235 mm, concentrated between July and September (Liu et al., 2017).



236 Fig. 1. The geographical location and sampling sites for rainfall, pond water, pore water, spring water,  
237 and fissure water in the Nianzhuang Catchment. The Nianzhuang Catchment is located in the hilly and  
238 gully region of the central Loess Plateau, with elevations ranging from 896 to 1269 m. The average depth  
239 of pore water wells is 8.0 ± 1.5 m (range: 4–10 m), while that of fissure water wells is 57.6 ± 29.2 m  
240 (range: 25–170 m). These sampling sites represent locations where both rainy and dry season samples  
241 were collected, and are all situated within the gully areas of the catchment.  
242

243  
244 The catchment features highly dissected loess terrain, with characteristic soils and landforms such  
245 as Loess Liang (ridges), Loess Mao (mounds), and steep loess slopes (Cai et al., 2019). Gullies often

删除了: 3

设置了格式: 字体颜色: 自动设置

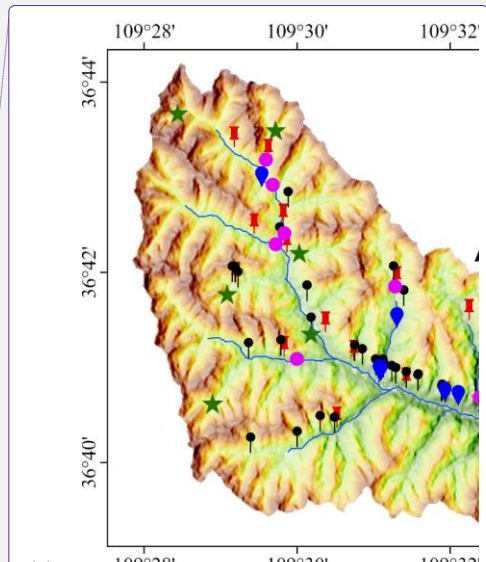
带格式的: 标题 3

删除了: he

删除了: —

删除了: —

删除了: 2



删除了: 109°28' 109°30' 109°32'

删除了: 2

删除了: catchment

删除了: catchment

删除了: 869

设置了格式: 字体颜色: 自动设置

删除了:

删除了: —

258 “V”- or “U”-shaped, dominate the lower-lying regions and serve as important recharge zones. These  
 259 landforms, together with ancient landslides, minor collapses, and sinkholes, highlight the geomorphic  
 260 instability of the Loess Plateau landscape (Li et al., 2021). From May to October 2023, total rainfall  
 261 reached 420 mm, with 115 mm in September alone. Despite this substantial precipitation, field  
 262 observations revealed shallow infiltration depths on loess slopes even after heavy rainfall events of up to  
 263 41 mm. Infiltration was limited to 20–30 cm at hilltops and about 80 cm at mid-slope, with no distinct  
 264 preferential flow and largely unsaturated soil profiles (Fig. 2). These observations suggest that  
 265 groundwater recharge occurs mainly through surface or near-surface runoff converging into engineered  
 266 gully systems, underscoring their critical role as focused zones of groundwater recharge and key sites for  
 267 studying these processes.

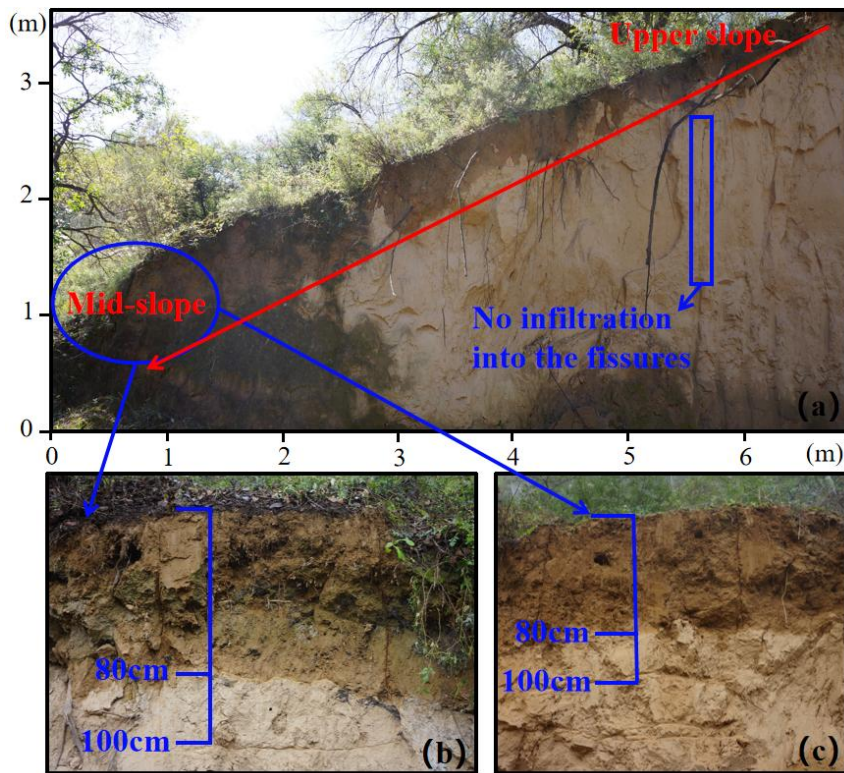
删除了：—

删除了：

删除了：gullies

删除了：natural

带格式的：居中



268  
 269 Fig. 2. The topographic profile of the Nianzhuang Catchment in the hilly region of the Loess Plateau.  
 270 Full profile from the top to mid-slope (a); two repeated mid-slope profiles (b, c). The photo was taken  
 271 after a 41 mm rainfall event over four days. Subsequent measurements showed that infiltration depths

276 reached only 20–30 cm at the top of the slope, compared to approximately 80 cm at the mid-slope  
277 positions.

278

279 The stratigraphy of the catchment reflects the typical layered structure of the Loess Plateau, which  
280 plays a key role in controlling groundwater recharge. In upland hilly areas, thick loess deposits overlie  
281 bedrock, with the Upper Pleistocene Malan Loess, a light grayish-yellow, loosely textured, and silt-rich  
282 unit (>60%), characterized by well-developed vertical joints and abundant hematite and goethite.

283 Beneath it lies the Middle Pleistocene Lishi Loess, a grayish-yellow to light brown unit with prominent  
284 jointing and higher iron mineral content. Below the loess, the Neogene Red Clay appears as a distinctly  
285 reddish, calcareous nodule-bearing aquitard due to its low permeability. The entire sequence rests on  
286 Jurassic sandstone–conglomerate bedrock, composed mainly of quartz-rich fluvial–lacustrine deposits.

287 Loess thickness in the Liang and Mao regions often exceeds 150 meters, resulting in deep water  
288 tables and limited groundwater accessibility. In contrast, gully zones exhibit distinctly different  
289 hydrogeological characteristics. Here, thinner loess layers overlie Neogene and Jurassic formations,  
290 sometimes interbedded with coal seams up to 5 meters thick (Fig. 3a–c). The significant reduction in  
291 loess thickness, combined with the relatively high permeability of Neogene coarse sandstone and  
292 conglomerate (0.07–0.31 m/d), creates favorable conditions for infiltration and focused recharge. These  
293 dynamics are especially evident at gully heads, where surface runoff from adjacent uplands converges  
294 and infiltrates, forming efficient recharge zones. As a result, gully areas tend to have shallower water  
295 tables and more rapid water renewal, making them more suitable for domestic groundwater use. Springs  
296 frequently emerge at gully bottoms where lateral flow is facilitated at the loess–bedrock interface.  
297 Streams in this dry environment are largely intermittent.

删除了:  
带格式的: 缩进: 首行缩进: 2 字符

删除了:—

删除了:—

删除了: (value range)

删除了:.

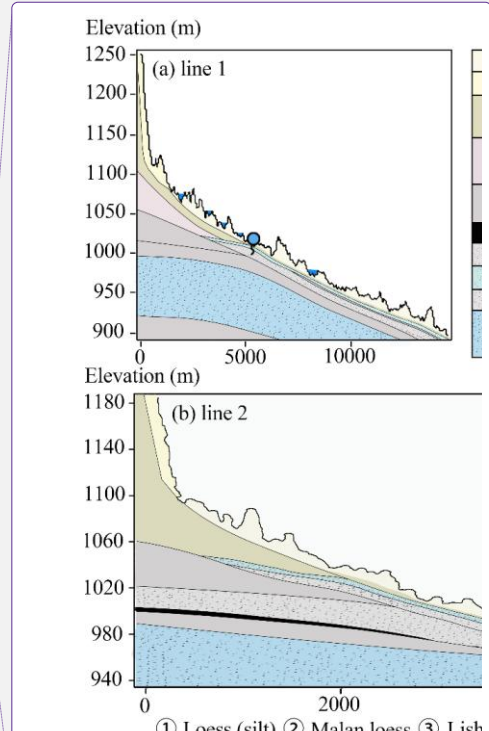
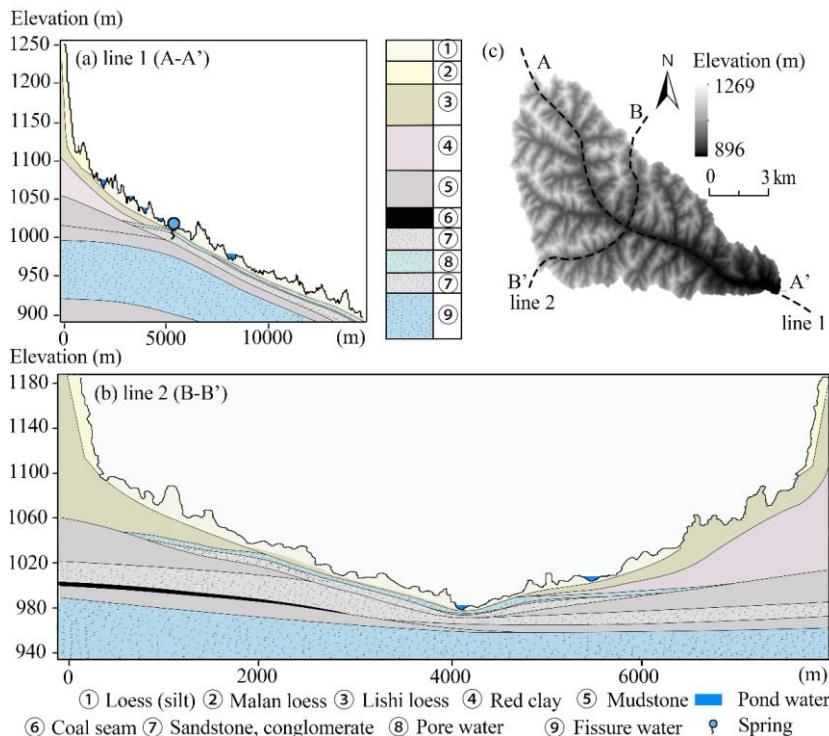
删除了: 3a

删除了:—

删除了: 7.5–36.19

删除了:—

删除了:



309 Fig. 3. Hydrogeologic cross-section of the study area. Cross-section along Line 1 (Northwest-Southeast)

311 (a); cross-section along Line 2 (Southwest-Northeast) (b); location map of Line 1 and Line 2 within  
 312 the study area (c). The Malan Loess (11.7–12.6 Ka BP) and Lishi Loess (12.6–78.1 Ka BP) are two major  
 313 Quaternary loess stratigraphic units in China. Based on hydrogeological research, the stratigraphy of the  
 314 hilly region features a multi-layer structure from top to bottom: Upper Pleistocene Malan Loess, Middle  
 315 Pleistocene Lishi Loess, Neogene Red Clay and Mudstone (2.58–23.03 Ma BP), and Jurassic Sandstone  
 316 and Conglomerate (145–201.3 Ma BP). In the gully region, the stratigraphy includes Holocene loess (silt,  
 317 11.7 ka BP–present), Middle Pleistocene Lishi Loess, Neogene sandstone and mudstone, and Jurassic  
 318 sandstone and conglomerate, with some areas containing coal seams up to 5 meters thick.

319  
 320 Groundwater in the catchment can be broadly categorized into three types: pore water, spring water,  
 321 and fissure water. Pore water is stored in permeable sandstone and conglomerate aquifers beneath loess  
 322 and above mudstone or red clay. These aquifers are approximately 2–3 m thick, exhibit a sheet-like  
 323 distribution, and have low water yield. Conceptually, “pore water” here refers to groundwater in a

删除了: ⑥ Coal seam ⑦ Sandstone, conglomerate (

带格式的: 居中

删除了: 3

设置了格式: 字体: 非倾斜

设置了格式: 字体: 10 磅

设置了格式: 字体: 10 磅

设置了格式: 字体: 10 磅

326 saturated aquifer, not to soil moisture. Fissure water occurs in fractured bedrock aquifers, which are  
327 spatially discontinuous due to irregular fracture development. The main water-bearing zones include  
328 cavities and jointed fissure networks, with an average aquifer thickness of about 6 m and moderate water  
329 yield. Hydraulic conductivity in these sandstone and conglomerate aquifers ranges from 0<sub>v</sub> to 0.47 m/d  
330 (Cai et al., 2019). Spring water emerges primarily at gully bases, especially in upper catchments, and  
331 originates from both pore and fissure sources, possibly supplemented by surface or pond water. Springs  
332 fed by pore water typically have low discharge rates (0–0.1 L/s) and low water yield, while those fed by  
333 fissure water exhibit moderate discharge rates (0.5–1.0 L/s) and moderate water yield.

334 Over recent decades, landscape rehabilitation through the Grain for Green Project and land  
335 reshaping under the Gully Land Consolidation Project have significantly altered the hydrological regime  
336 (Fu et al., 1999; Liu et al., 2017). Historically, surface runoff in the degraded catchment was flashy and  
337 episodic due to sparse vegetation. However, ecological restoration and small-scale engineering  
338 interventions, such as check dams, terraces, roads, and ponds, have moderated surface hydrology. Surface  
339 runoff, generated primarily during storm events, now contributes alongside delayed baseflow from  
340 groundwater recharge and interflow. The latter is often limited by the thick unsaturated zone in upland  
341 loess areas but may be enhanced in gully regions, where stratigraphy and land use favor infiltration  
342 (Wang et al., 2024; Gates et al., 2011). Gully areas also contain numerous check dams and ponds, with  
343 most water sourced from Hortonian overland flow of slope lands and direct rainfall. These small water  
344 bodies, often constructed for erosion control and water retention, influence local hydrological dynamics  
345 and may play a role in enhancing infiltration and recharge.

### 347 3. Methods

348 Our approach integrates stable isotope analysis ( $\delta^2\text{H}$  and  $\delta^{18}\text{O}$ ), chloride concentration analysis, and  
349 water table fluctuation monitoring to investigate groundwater recharge dynamics. The isotopic  
350 composition of water bodies reflects both their origins and the processes they undergo, such as  
351 evaporation, infiltration, and mixing (Wan and Liu, 2016; Kumar et al., 2019; Dasgupta et al., 2024).  
352 Precipitation, surface water, and groundwater typically exhibit distinct isotopic signatures due to these  
353 differing pathways (Gleeson et al., 2016; Kuang et al., 2019; Al-Oqaili et al., 2020). When isotopic  
354 patterns among water sources converge, it often indicates strong hydrological connectivity (Yang and

设置了格式: 字体: 10 磅

删除了: Fissure water occurs within fractured bedrock aquifers but is spatially discontinuous due to irregular fissure development.

删除了: .0218

删除了: 1

删除了: ay

删除了: —

删除了: —

设置了格式: 字体: 10 磅

设置了格式: 字体: 10 磅

设置了格式: 字体: 10 磅

设置了格式: 字体: 10 磅

设置了格式: 字体: 10 磅

删除了: —

删除了: —

删除了: 4

设置了格式: 字体颜色: 自动设置

带格式的: 标题 3

删除了: —

367 Wang, 2023). Because stable isotopes behave conservatively, they serve as effective tracers of water  
368 sources and flow paths (Gleeson et al., 2016; Al-Oqaili et al., 2020; Dasgupta et al., 2024). In parallel,  
369 water table fluctuation (WTF) monitoring provides a means of estimating recharge by observing changes  
370 in groundwater levels in response to precipitation events (Nachabe, 2002; Heppner and Nimmo, 2005;  
371 Gumuła-Kawęcka et al., 2022). By combining these complementary methods, this study aims to elucidate  
372 groundwater recharge pathways and quantify recharge rates in gully regions, thereby identifying key  
373 recharge zones and advancing our understanding of groundwater processes in the Loess Plateau.

374

### 375 3.1. Field measurements of hydrological data

376 Precipitation was collected from October 24, 2023, to October 24, 2024, using a weather station  
377 situated in an open field within the catchment. Continuous groundwater level data were recorded from  
378 September 24, 2023, to December 20, 2024. Groundwater pressure and temperature were monitored  
379 using Onset HOBO U20-001-03 sensors (20 m range), with a pressure accuracy of  $\pm 0.3\%$  FS ( $\pm 2.55$  kPa)  
380 and a resolution of  $< 0.085$  kPa, and a temperature accuracy of  $\pm 0.44$  °C with a resolution of 0.1 °C. The  
381 sensor was calibrated to atmospheric pressure before installation to ensure accurate measurement of  
382 absolute static water pressure, and water table levels were calculated based on the measured pressure  
383 data. The conversion relationship between water pressure and groundwater level is given by  $Y =$   
384  $0.86 \times X - 22.1$  where  $Y$  represents the groundwater level and  $X$  represents the water pressure. The  
385 conversion between water pressure and groundwater level is based on the principle of hydrostatics. The  
386 hydrostatic pressure  $P$  at the sensor is related to the height of the overlying water column  $h$  by  $P = \rho gh$ ,  
387 where  $\rho$  is the water density and  $g$  is the gravitational acceleration. In unconfined aquifer, the pressure  
388 measured by the sensor corresponds directly to the static pressure exerted by the overlying water column.  
389 From this, the water column height  $h$  can be calculated, and combined with the sensor's installation  
390 elevation, the depth to the groundwater table can be determined. Notably, the monitoring well is located  
391 in the pore water layer of the gully region. The well is hand-dug (1.1 m wide, 10 m deep) and is unaffected  
392 by human activities.

393 Soil physical properties were assessed using the cutting ring method, based on undisturbed soil cores  
394 collected at five depth intervals: 0–10, 10–20, 20–30, 30–40, and 40–50 cm. Quadruplicate samples were  
395 taken near groundwater monitoring wells in the gully using pre-weighed cutting cylinders. The samples  
396 were immediately transported to the laboratory for analysis. Bulk density, capillary porosity, non-

删除了:—

删除了:4

删除了:,

设置了格式: 字体: (默认) Times New Roman

设置了格式: 字体: (默认) Times New Roman

400 capillary porosity, total porosity, and field water capacity were determined following the LY/T 1215-  
401 1999 standard for forest soil water-physical properties. Soil particle size distribution was analyzed using  
402 a laser particle size analyzer at the College of Natural Resources and Environment, Northwest A&F  
403 University. Soil texture classification followed the USDA system: sand (0.05–2 mm), silt (0.002–0.05  
404 mm), and clay (<0.002 mm) (Dane et al., 2002).

405

### 406 3.2 Water sampling

407 A total of 181 water samples were collected from various locations in rainy season (September 2023,  
408 99 samples) and dry season (April 2024, 82 samples); see Fig. 1. Rainy season samples included 48 from  
409 rainfall, 7 from pond water (water retention reservoirs), 9 from spring water, 9 from pore water, and 26  
410 from fissure water. During the dry season, samples included 31 from rainfall, 6 from pond water, 8 from  
411 pore water, 29 from fissure water, and 8 from spring water.

412 Pore water was collected from several shallow, hand-dug wells measuring approximately 1.1 meters  
413 in diameter and 4–10 meters in depth. Fissure water was sampled from deeper, narrow-diameter wells  
414 (0.2 meters wide, 25–170 meters deep). In areas with numerous deep wells, we employed random  
415 sampling to ensure representative coverage of fissure water sources. To minimize the risk of collecting  
416 stagnant water, all pore and fissure water wells were purged for 10–15 minutes prior to sampling. Spring  
417 water was collected directly from natural discharge points, although most springs in the region exhibit  
418 low flow rates, typically less than 0.1 L/s, occasionally reaching up to 0.2 L/s.

419 A total of 18 bulk rainfall collectors were randomly and evenly distributed across the 54 km<sup>2</sup> study  
420 area, and samples were collected immediately following rainfall events. For nighttime precipitation,  
421 samples were collected the next morning at 6:00 AM. During the study period, we collected two types of  
422 precipitation samples: (1) spatial samples from individual events (18 in the rainy season and 15 in the  
423 dry season) across the catchment, capturing spatial variability; and (2) sequential events at a fixed station  
424 (30 in the rainy season and 16 in the dry season), characterizing seasonal inputs.

425 During sampling, 100 mL collection bottles were rinsed two to three times with the sample water,  
426 then slowly filled to minimize air exposure. After filling, the bottles were tightly sealed with screw caps  
427 and further secured with Parafilm to prevent evaporation and contamination. All samples were  
428 immediately stored in a portable cooler at 4°C and transported to the laboratory for isotopic and chloride  
429 concentration analysis.

删除了: 4

删除了: 2

删除了: —

433

### 434 3.3. Isotopic analysis

435 The  $\delta^2\text{H}$  and  $\delta^{18}\text{O}$  values of the water samples were determined using a Los Gatos Research liquid  
436 water isotope analyzer (Model 912-0032, LGR Inc., California, USA) at the Institute of Water-Saving  
437 Agriculture in Arid Areas of China, Northwest A&F University. Each sample was injected six times in  
438 the following sequence: three standard injections, followed by six natural sample injections, and then  
439 three additional standard injections. The isotope ratios were calculated using the average composition  
440 from injections 4 through 6.

441 Isotope values are expressed in delta ( $\delta$ ) notation, which represents the relative difference in isotope  
442 ratio between a sample and the Vienna Standard Mean Ocean Water (VSMOW) reference. The  
443 measurement precision was  $\pm 0.5\text{‰}$  for  $\delta^2\text{H}$  and  $\pm 0.1\text{‰}$  for  $\delta^{18}\text{O}$ . The delta values were calculated using  
444 the following equations:

$$445 \quad \delta^{18}\text{O} = \left( \frac{R_{\text{sample}}}{R_{\text{standard}}} \right) - 1 \quad (1)$$

$$446 \quad \delta^2\text{H} = \left( \frac{R_{\text{sample}}}{R_{\text{standard}}} \right) - 1 \quad (2)$$

447 where  $R_{\text{sample}}$  and  $R_{\text{standard}}$  are the ratios of heavy to light isotopes ( $^{18}\text{O}/^{16}\text{O}$  or  $^2\text{H}/^1\text{H}$ ) in the sample  
448 and the standard, respectively. Results are expressed in per mil (‰).

449

### 450 3.4. Mixing process of different water bodies

451 Inverse transit time proxies (ITTPs) were calculated to assess differences in water transit times and  
452 mixing processes across various water bodies (Tetzlaff et al., 2009). ITTPs are defined as the ratio of the  
453 standard deviation of  $\delta^{18}\text{O}$  in the water sample (e.g., pond water, spring water, pore water, or fissure  
454 water) to that in precipitation over the same time period:

$$455 \quad \text{ITTP} = \frac{\sigma_{\delta^{18}\text{O}}(\text{sample})}{\sigma_{\delta^{18}\text{O}}(\text{precipitation})} \quad (3)$$

456 This ratio captures the attenuation of seasonal isotopic variability in  $\delta^{18}\text{O}$  as water moves through  
457 the landscape. In general, ITTP values less than 1 indicate substantial damping of the precipitation signal,  
458 consistent with longer water residence times, greater mixing, and larger storage volumes. Conversely,  
459 values approaching 1 suggest minimal damping and rapid flow paths.

460 However, interpretation of ITTPs must also account for fractionation processes. In particular,  
461 evapotranspiration (ET) selectively removes lighter isotopes ( $^{16}\text{O}$ ), enriching the remaining water in

删除了: 4

删除了: 4

删除了: —

465 heavier isotopes ( $^{18}\text{O}$ ). This enrichment can artificially increase the variance of  $\delta^{18}\text{O}$  in near-surface or  
466 shallow soil water compartments, inflating ITTP values even in systems with relatively slow transit times  
467 (Tetzlaff et al., 2009). This is especially relevant in arid and semi-arid regions, where ET can dominate  
468 the water balance during dry seasons.

469

### 470 3.5. Hydraulic connectivity estimation

471 [Structural Equation Modeling \(SEM\) has been widely applied in water science to evaluate complex](#)  
472 [relationships among hydrological, geological, and anthropogenic variables, particularly in studies of](#)  
473 [groundwater contamination and water quality degradation \(Wu, 2010; Lupi et al., 2019; Xie et al., 2025\).](#)  
474 [In this study, SEM is used explicitly as an exploratory, hypothesis-generating tool to assess potential](#)  
475 [hydrological connectivity among water sources based on dual-isotope \( \$\delta^2\text{H}\$ – \$\delta^{18}\text{O}\$ \) data from rainfall,](#)  
476 [pond water, spring water, pore water, and fissure water. SEM is not a mass-conserving or process-based](#)  
477 [flow model, nor is it used here to infer volumetric fluxes, recharge rates, or source apportionment. Instead,](#)  
478 [it serves as a statistical consistency check on hypothesized connectivity, identifying direct and indirect](#)  
479 [associations among water bodies that are evaluated in conjunction with tracer evidence and hydrometric](#)  
480 [observations.](#)

481 [Within the SEM framework, path relationships are primarily explained through two types of effects:](#)  
482 [The direct effect refers to the immediate impact of one variable on another through a single path, typically](#)  
483 [quantified as a standardized regression coefficient. Total effect represents the overall impact of one](#)  
484 [variable on another through all possible paths \(including both direct and indirect\), calculated as the sum](#)  
485 [of the direct effect and all indirect effects. Comparing direct and total effects allows identification of](#)  
486 [intermediary linkages and dominant association structures within the hypothesized connectivity network.](#)

487 Given the potential for isotopic signatures to be altered by evaporation, mixing, or other non-  
488 conservative processes, results must be interpreted with caution. Pathways with p-values > 0.05 were  
489 excluded during model refinement, and the final model met standard goodness-of-fit criteria (degrees of  
490 freedom < 3, RMSEA < 0.05, CFI > 0.95, NFI > 0.95). SEM analysis was conducted using SPSS Amos  
491 26.0 (IBM SPSS, Chicago, Illinois, USA).

492 In addition, we applied variance partitioning to evaluate the relative contributions of different water  
493 sources to pore and fissure water. This method decomposes the total variance in isotopic composition  
494 into components attributable to individual sources (e.g., precipitation, pond water, spring water), offering

删除了: 4

删除了: Structural Equation Modeling (SEM) has been widely applied in water science to evaluate complex causal relationships among hydrological, geological, and anthropogenic variables—, particularly in studies of groundwater contamination and water quality degradation (Wu, 2010; Lupi et al., 2019; Xie et al., 2025). In this study, we adapted SEM as an exploratory framework to assess hypothesized recharge linkages among water sources, using dual-isotope ( $\delta^2\text{H}$ – $\delta^{18}\text{O}$ ) data from rainfall, pond water, spring water, pore water, and fissure water. Although SEM is not a mass-conserving approach and is less commonly used in isotope-based flowpath analysis, it enables estimation of statistically significant relationships and indirect linkages within a hypothesized recharge system.

设置了格式: 字体: 非加粗

设置了格式: 字体: 非加粗

删除了: Interpreted cautiously and in combination with independent indicators, these results provide quantitative support for relative connectivity patterns, rather than definitive evidence of causal flow paths or recharge magnitudes.

删除了: By comparing the direct and total effects, the complex causal network and interaction strength between variables can be systematically revealed, providing a quantitative basis for understanding hydrological processes.

设置了格式: 突出显示

519 a complementary estimate of source influence. [While useful, this approach remains subject to the same](#)  
520 [limitations as SEM, particularly the challenges of isotopic overlap and limited resolution in environments](#)  
521 [affected by mixing and evaporation \(Lai et al., 2022\).](#)

522 To further constrain recharge pathways, we incorporated chloride ion (Cl<sup>-</sup>) as a conservative tracer.  
523 Unlike stable isotopes, [Cl<sup>-</sup> behaves conservatively with respect to fractionation, and when interpreted](#)  
524 [alongside isotopes, it can further explain mixing and recharge pathways.](#) Chloride concentrations in all  
525 water samples were analyzed using an ion chromatograph (DIONEX ICS-1100) at the College of Natural  
526 Resources and Environment, Northwest A&F University, China. Each sample was analyzed in triplicate,  
527 with charge balance errors maintained below 5% to ensure analytical accuracy. This rigorous approach  
528 enhances the reliability of chloride data, supporting its integration with isotopic indicators in source  
529 attribution.

### 531 3.6. Groundwater recharge

532 Groundwater recharge in the gully zone is quantified using the water table fluctuation (WTF)  
533 method, which infers recharge and discharge events from temporal changes in groundwater levels (Healy  
534 and Cook, 2002; Gumuła-Kawęcka et al., 2022). We recognize that recharge can originate from three  
535 hydrological sources: (1) surface water; (2) the unsaturated zone (3) and the saturated zone (Scanlon et  
536 al., 2022; Wang et al., 2024). Among these, estimates based on the saturated zone are generally most  
537 reliable, as recharge from the unsaturated zone reflects potential inputs that may never reach the water  
538 table (Beven and Germann, 2013; Huang et al., 2019). The WTF method is widely used for estimating  
539 saturated zone recharge due to its high temporal resolution and conceptual simplicity (Xu et al., 2024).  
540 Based on previous site-specific studies (Wang et al., 2024), this method is well-suited for our analysis.

541 The water table fluctuation method assumes that changes in the groundwater table result solely from  
542 recharge or discharge, assuming a constant specific yield (S<sub>y</sub>) over time (Healy and Cook, 2002; Obuobie  
543 et al., 2012). The formula is as follows:

$$544 R_i = S_y \frac{\Delta H_i}{\Delta t} \quad (4)$$

545 where, *R* is the groundwater recharge (mm), *S<sub>y</sub>* is the specific yield of the aquifer,  $\Delta H_i$  (where  
546  $\Delta H_i > 0$ ) is [rise in groundwater level between days \*i\* - 1 and \*i\*, and  \$\Delta t\$  is the time interval \(one day\).](#)  
547 Specific yield, which [represents effective drainable porosity of the shallow gully aquifer system,](#) rather

删除了:—

删除了: While useful, this approach remains subject to the same limitations as SEM—particularly the challenges of isotopic overlap and limited resolution in environments affected by mixing and evaporation (Lai et al., 2022).

删除了: but its concentration can increase under evaporation and decrease under dilution;

删除了: still constrain

删除了: chloride is unaffected by evaporation or biological processes, making it a robust indicator for identifying recharge sources and tracking subsurface water movement

删除了: 4

删除了: the groundwater table ris

删除了: e caused by recharge

删除了: y

删除了: *t* is time period

删除了: represents the proportion of water that drains freely from the saturated zone under gravity

566 than soil water release from the unsaturated zone. In this study,  $S_y$  was estimated using two  
567 complementary approaches: (1) an empirical method based on soil texture to constrain plausible ranges  
568 of drainable porosity, and (2) the test pit method, in which  $S_y$  is calculated as the difference between total  
569 porosity and field water capacity (Liang, 2016). These approaches provide an estimate of aquifer-scale  
570 effective specific yield appropriate for shallow unconfined groundwater systems in loess-derived gully  
571 environments.

572 Empirical values for soil texture are referenced in Table A1. The test pit method for estimating  $S_y$  is  
573 described as follows:

$$574 S_y = TP - FWC \quad (5)$$

575 where,  $TP$  (total porosity) and  $FWC$  (field water capacity) were measured using the cutting ring  
576 method.

577 We applied two methods to calculate the daily groundwater table increments ( $\Delta H_i$ ). The RISE  
578 method assumes that recharge occurs only when the groundwater table elevation increases between two  
579 consecutive days (Gumula-Kawęcka et al., 2022). Thus,  $\Delta H_i = H_i - H_{i-1}$  if  $H_i > H_{i-1}$ , otherwise,  
580  $\Delta H_i = 0$ . The master recession curve (MRC) method assumes that, in the absence of recharge, the  
581 groundwater table declines daily by a specific amount ( $\Delta H_{MRCi}$ ). This amount represents a simplified  
582 approximation of discharge processes in the aquifer, particularly lateral outflow to nearby surface water  
583 bodies. MRC establishes a functional relationship between a daily decrement of the water table ( $\Delta H_{MRCi}$ )  
584 and the water table elevation ( $H_{i-1}$ ) during periods without recharge.

$$585 \Delta H_{MRCi} = A \cdot H_{i-1} + B \quad (6)$$

586 where, the coefficients A and B were fitted for each piezometer based on data from periods of  
587 continuous groundwater table decreases lasting longer than two weeks. The daily water table increment  
588 due to recharge was then calculated as:  $\Delta H_i = H_i - H_{i-1} + \Delta H_{MRCi}$  if  $H_i > (H_{i-1} - \Delta H_{MRCi})$ ,  
589 otherwise,  $\Delta H = 0$ .

590 Notably, we used water dynamics from October 24, 2023, to October 24, 2024, to calculate pore  
591 water recharge, as this period exhibited clear groundwater fluctuations, making it more representative.

592

## 593 **4. Results**

### 594 **4.1. Soil properties**

删除了: ,

删除了: determined

删除了: methods: the soil texture empirical method and the test pit method (Liang, 2016).

删除了: 5

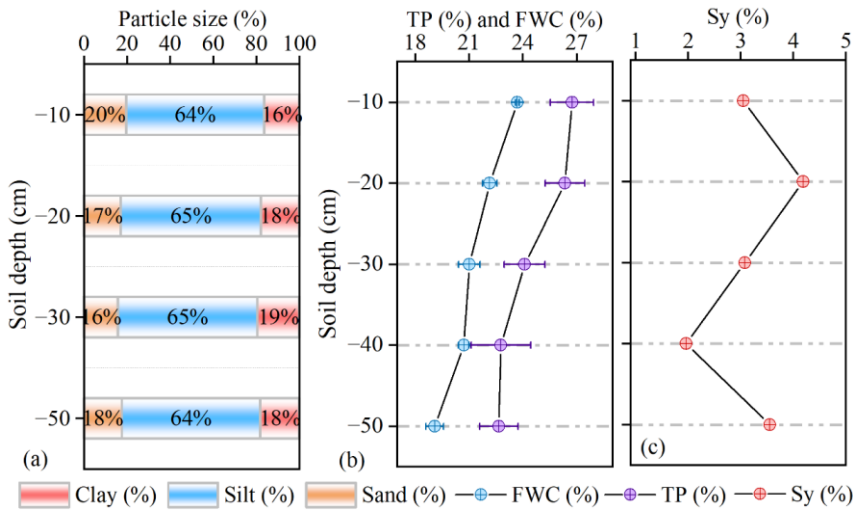
设置了格式: 字体颜色: 自动设置

带格式的: 标题 3

删除了: 5

601 The upper 50 cm of the soil profile is composed primarily of silt ( $64.6 \pm 0.6\%$ ), with smaller but  
 602 nearly equal proportions of clay ( $18.0 \pm 1.3\%$ ) and sand ( $17.4 \pm 1.6\%$ ), classifying the loess as silt loam  
 603 according to the International Union of Soil Sciences (IUSS) scheme (Fig. 4a). Total porosity and field  
 604 water capacity decreased slightly with depth, averaging  $24.5 \pm 1.9\%$  and  $21.3 \pm 1.7\%$ , respectively (Fig.  
 605 4b). Specific yield remained relatively consistent within the 10–50 cm depth interval, averaging  
 606  $3.2 \pm 0.8\%$ , falling within the expected empirical range for silt loam soils (2%–7%) (Fig. 4c).

删除了: %--



607 Clay (%) Silt (%) Sand (%) FWC (%) TP (%) Sy (%)

608 Fig. 4. Vertical variation in soil texture and water retention characteristics in the gully region of the Loess  
 609 Plateau. (a) Soil particle size distribution by depth, showing relatively uniform composition across layers  
 610 (10–50 cm), dominated by silt (64–65%), with moderate clay (16–20%) and low sand (16–20%) content.  
 611 This fine-textured profile supports high moisture retention and slows infiltration, promoting delayed  
 612 recharge. (b) Depth profiles of total porosity (TP) and field water capacity (FWC) reveal decreases with  
 613 depth to 40 cm, with FWC reaching ~27%, suggesting greater water-holding capacity in subsoil layers  
 614 and enhanced buffering of infiltrated water. (c) Vertical variations in the Specific Yield (Sy) across  
 615 different soil layers. Collectively, these physical properties reflect a vertically stratified soil system where  
 616 near-surface layers regulate infiltration pulses, and deeper layers act as long-term storage, shaping the  
 617 timing and magnitude of subsurface recharge.

删除了: increases

删除了:

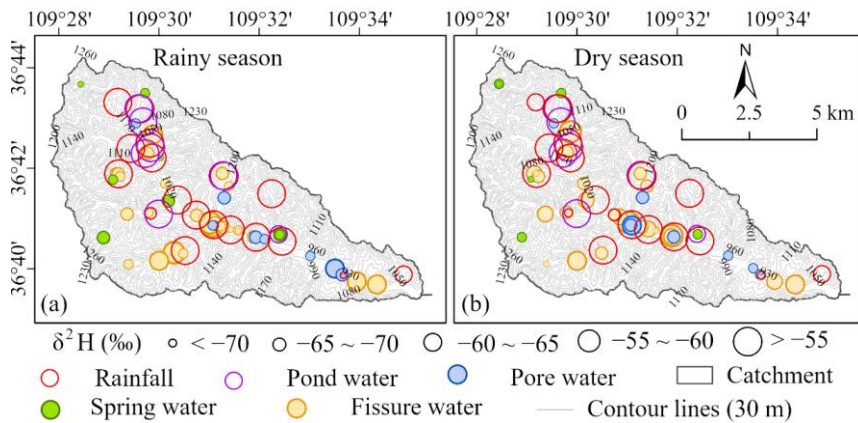
删除了: Specific yield (Sy) peaks at -20 cm (4.5%) but decreases with depth, indicating shallower layers are more responsive to infiltration and release, while deeper layers tend to store water with minimal drainage.

618  
 619 **4.2. Hydrological signatures of rainfall, surface water, and groundwater sources**

删除了: 5

620 Pond water and rainfall exhibit similar spatial isotopic patterns, with more positive  $\delta^2\text{H}$  values ( $\delta^2\text{H} >$

629  $-55\text{‰}$ ) than spring water, pore water, and fissure water (Fig. 5a, b). These values are line with the notion  
 630 of direct rainfall and Hortonian runoff are the primary source of pond water. In contrast, the  $\delta^2\text{H}$  values  
 631 of pore, spring, and fissure water show little seasonal variation and are consistently more negative ( $\delta^2\text{H}$   
 632  $< -55\text{‰}$ ), than mean rainfall, indicating longer residence times and reduced evaporative influence.



633 Fig. 5. The spatial distributions of  $\delta^2\text{H}$  values during the (a) rainy season and (b) dry season for rainfall,  
 634 pond water, spring, pore water, and fissure water in the gully region of the Loess Plateau. To highlight  
 635 spatial differences among water sources,  $\delta^2\text{H}$  values were classified into five intervals:  $< -70\text{‰}$ ,  $-70$  to  
 636  $-65\text{‰}$ ,  $-65$  to  $-60\text{‰}$ ,  $-60$  to  $-55\text{‰}$ , and  $> -55\text{‰}$ . Sampling points are color-coded by water type: red  
 637 for rainfall, purple for pond water, blue for pore water, green for spring water, and orange for fissure  
 638 water.  
 639 water.

641 The  $\delta^2\text{H}$ – $\delta^{18}\text{O}$  relationships and box plots for each water source reveal key insights into the  
 642 dominant hydrological processes occurring during the rainy season (Fig. 6). Firstly, rainfall follows a  
 643 Local Meteoric Water Line (LMWL) of  $\delta^2\text{H} = 7.7 \cdot \delta^{18}\text{O} + 8.9$  ( $R^2 = 0.95$ ), which is closely aligned, though  
 644 slightly offset, from the Global Meteoric Water Line (GMWL:  $\delta^2\text{H} = 8 \cdot \delta^{18}\text{O} + 10$ ) (rainy season; Fig. 6a,  
 645 c). This alignment indicates that precipitation in the region has a typical meteoric origin. Additionally,  
 646 minimal evaporative enrichment occurred prior to collection. The relatively wide interquartile range of  
 647 rainfall  $\delta^{18}\text{O}$  values suggests that precipitation was derived from storm systems with considerable  
 648 isotopic variability, reflecting differences in rainfall intensity, air mass origin, and temperature. However,  
 649 this variability remains moderate compared with global patterns that span extreme rainfall events and  
 650 broader climatic gradients.

删除了:—

删除了:—

删除了: (Kumar et al., 2019; Oqaili et al., 2020; Dasgupta et al., 2024)

655 Pond water, in contrast, exhibits a clear evaporation signature with a shallower slope of  $\delta^2\text{H} =$   
656  $5.6 \cdot \delta^{18}\text{O} - 17.1$  (rainy season;  $R^2 = 0.95$ ),  $\delta^2\text{H} = 4.6 \cdot \delta^{18}\text{O} - 20.7$  (dry season;  $R^2 = 0.74$ ). This signature  
657 aligns with expectations for surface water bodies, where open exposure facilitates fractionation. The box  
658 plot shows strong evaporative enrichment, with median values shifted significantly toward more positive  
659  $\delta^{18}\text{O}$  and  $\delta^2\text{H}$  compared to rainfall (Fig. 6a, c). Pond water maintains a relatively consistent slope and  
660 range across seasons, reinforcing its stable evaporative signature and less dynamic recharge behavior.

661 Spring water shows a clear seasonal transition in its isotopic composition. In the rainy season, its  
662 evaporation line ( $\delta^2\text{H} = 6.2 \cdot \delta^{18}\text{O} - 11.4$ ;  $R^2 = 0.75$ ) falls closer to the LMWL, suggesting that spring  
663 discharge is augmented by recent rainfall, likely delivered through rapid infiltration and shallow  
664 subsurface flow pathways during high-intensity events (Fig. 6a, b). However, the isotopic values of  
665 spring water are substantially more depleted than those of precipitation, indicating that older water stored  
666 in the porous subsurface aquifer dominates the overall spring flow composition composed of new and  
667 relatively old water.

668 During the dry season, the isotopic slope flattens and deviates further from the Local Meteoric Water  
669 Line (LMWL), reflecting increased evaporative influence or prolonged residence times (Fig. 6c, d). This  
670 seasonal shift suggests that as rainfall inputs decline, spring discharge becomes increasingly composed  
671 of slow-draining, older water that has undergone greater isotopic modification, either through mixing or  
672 evaporation in near-surface storage zones. Collectively, these patterns suggest that spring water acts as a  
673 dynamic integrator of recharge processes, rapidly responding to event-driven infiltration during the rainy  
674 season, yet also reflecting the delayed mobilization of older water stored in the subsurface. This behavior  
675 may be partly explained by a piston-like displacement mechanism, where incoming rainfall pushes pre-  
676 existing groundwater toward discharge zones.

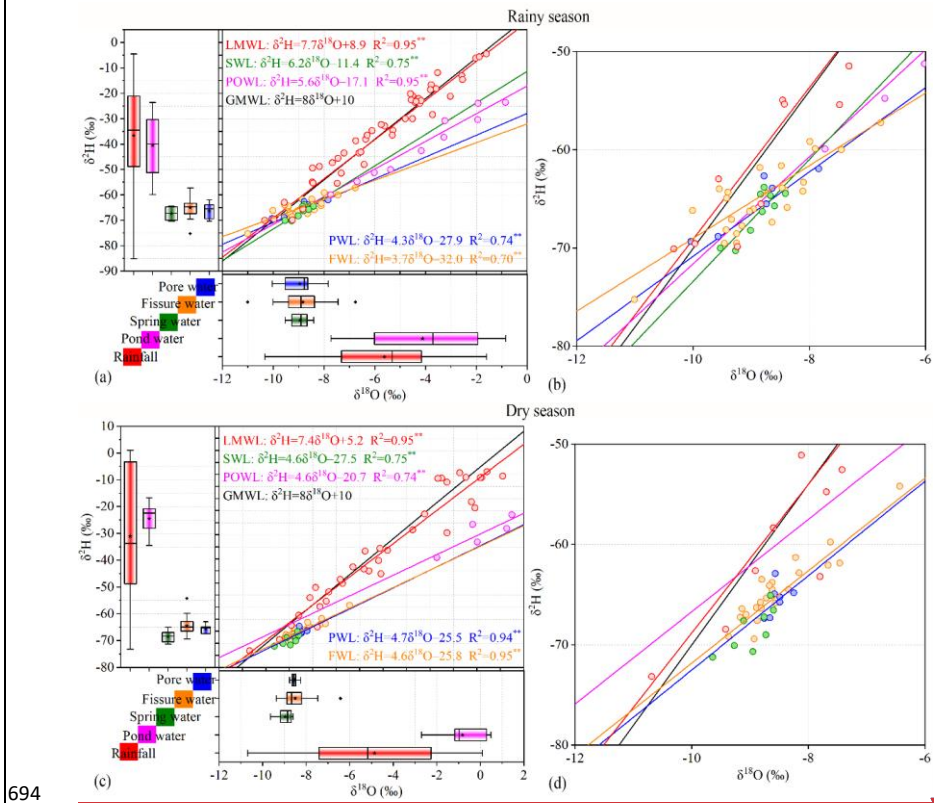
677 Pore and fissure water show remarkably similar isotopic signatures during the rainy season. Pore  
678 water, again sampled from a porous subsurface aquifer, follows a fitted line of  $\delta^2\text{H} = 4.3 \cdot \delta^{18}\text{O} - 27.9$   
679 (rainy season;  $R^2 = 0.74$ ), while fissure water, likely drawing from the same aquifer but through  
680 weathered bedrock pathways, fits  $\delta^2\text{H} = 3.7 \cdot \delta^{18}\text{O} - 32.0$  (rainy season;  $R^2 = 0.70$ ). These slopes are  
681 significantly flatter than those of rainfall, pond, or spring water, a pattern interpreted as evidence of  
682 evaporation prior to recharge or mixing with evaporated surface water. However, the box plots of the  
683 isotope data present a different picture. Both pore and fissure waters are systematically more depleted in  
684  $\delta^{18}\text{O}$  and  $\delta^2\text{H}$  than precipitation, and their narrow interquartile ranges suggest a relatively uniform

删除了:—

删除了:—

687 isotopic composition (Fig. 6a-d).

688 These depleted and uniform isotopic compositions indicate recharge dominated by isotopically light  
 689 rainfall events, primarily intense summer monsoon storms, rather than evaporative enrichment. Depleted  
 690 groundwater signatures thus reflect recharge from these summer events, with percolation delayed to  
 691 cooler seasons due to soil storage and reduced evaporation. The flat regression slopes and narrow  
 692 interquartile ranges are reconciled by longer residence times and mixing in the subsurface aquifer, which  
 693 acts as a hydrological buffer that dampens seasonal isotopic variability (Table A2).



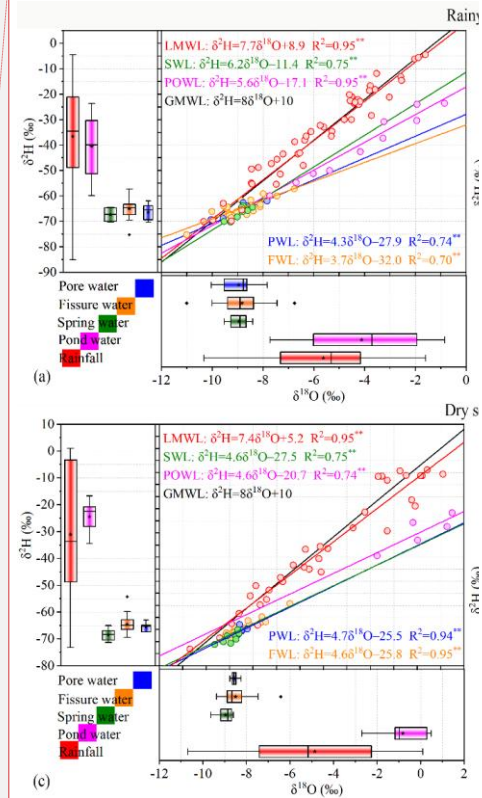
694 Fig. 6. Dual stable isotopic compositions of rainfall, pond water, spring water, pore water, and fissure  
 695 water during the rainy season and dry season in the gully region of the Loess Plateau. The black line  
 696 represents the global meteoric water line (GMWL,  $\delta^2\text{H}=10 + 8\delta^{18}\text{O}$ ). GMWL is the global meteoric water  
 697 line of Craig, LMWL is the local meteoric water line, SWL is the spring water line, POWL is the pond  
 698 water line, FWL is the fissure water line, and PWL is the pore water line. Panels (b) and (d) are magnified  
 699 views of (a) and (c), respectively, highlighting the isotopic compositions of pore water, fissure water, and  
 700

删除了:—

删除了:—

删除了: Rather than showing the enrichment expected from evaporation, these depleted and stable values point toward recharge dominated by a limited number of isotopically light rainfall events, such as early-season storms or high-altitude convective systems.

删除了:



删除了: (a)

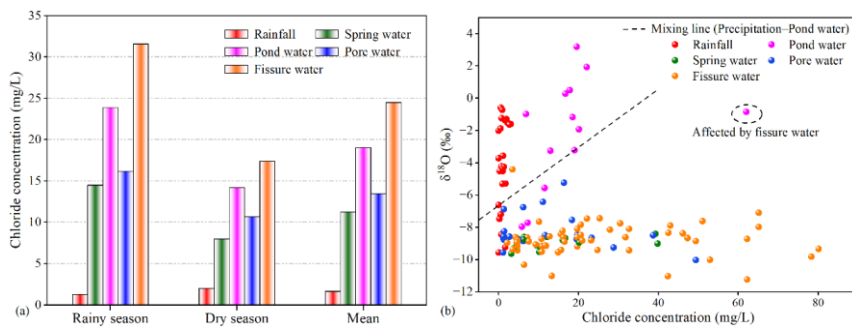
删除了: (b)

设置了格式: 上标

设置了格式: 上标

712 spring water (x-axis: -12 to -6‰; y-axis: -80 to -50‰).

713  
714 Complementing the isotope data, Cl<sup>-</sup> levels in pore water consistently fall between those of  
715 precipitation and pond water across both seasons (Fig. 7a), and the correlation pattern between chloride  
716 concentration and δ<sup>18</sup>O supports a mixed recharge origin for pore water (Fig. 7b). This trend aligns with  
717 the isotopic evidence from the rainy season and supports the interpretation that pond water contributes  
718 to pore water recharge via vertical percolation through the vadose zone, particularly during high-rainfall  
719 periods when infiltration capacity is exceeded.



720  
721 **Fig. 7. Chloride concentration of various water sources in the rainy and dry seasons (a), and the spatial**  
722 **relationship between chloride concentration and δ<sup>18</sup>O for different water sources (b).**

723  
724 The inverse transit time proxies (ITTPs) broadly support the dual-isotope interpretations of water  
725 source dynamics. Pond water exhibited the highest ITTP values ( $1.5 \pm 0.7$ ), indicating rapid turnover and  
726 limited subsurface storage. These elevated values likely reflect inputs from direct rainfall and overland  
727 flow, as well as evaporative enrichment, which increases isotopic variability and can artificially shorten  
728 the apparent residence time. In contrast, pore water ( $0.7 \pm 0.3$ ) and fissure water ( $0.6 \pm 0.5$ ) showed lower  
729 ITTPs, consistent with longer residence times, greater subsurface mixing, and attenuation of seasonal  
730 isotopic signals due to delayed recharge. Spring water had the lowest ITTPs ( $0.3 \pm 0.2$ ), reflecting slow  
731 subsurface transport and integration of older water sources (Fig. 8).

删除了: ...

Complimenting

带格式的: 缩进: 首行缩进: 0 字符

删除了: Complimenting

删除了: A2

删除了:

删除了: supporting

删除了: The lack of a similar isotopic pattern in the dry season likely reflects stronger evaporative enrichment of pond water, which masks its potential contribution to pore water recharge in dual-isotope space.

带格式的: 缩进: 首行缩进: 0 厘米

删除了: . While these patterns align with conceptual expectations of residence time and flow path length, the limited number of samples—particularly for pond, spring, and pore water—warrants caution in interpreting seasonal dynamics ...

删除了: 7

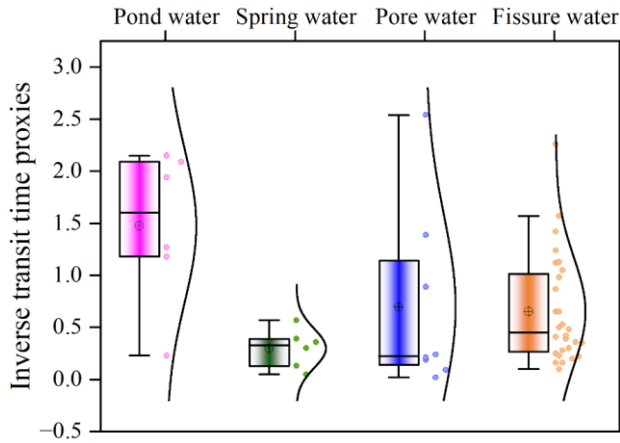


Fig. 8. Boxplots and kernel density estimates of inverse transit time proxies (ITTPs) for pond water, spring water, pore water, and fissure water. Higher ITTP values indicate shorter water transit times since precipitation, while lower values suggest longer residence and greater isotopic damping. Pond water exhibited the highest and most consistent ITTPs (median  $\approx 1.5$ ), implying rapid recharge from recent rainfall or stormflow. Spring water showed the lowest ITTPs ( $\approx 0.3$ ), consistent with longer subsurface flow paths and storage. Pore and fissure water displayed intermediate and more variable ITTPs, reflecting mixing between recent and older water sources, as well as seasonal differences in infiltration and soil moisture replenishment.

#### 4.3. Hydrological linkages and recharge efficiency

The SEM analysis reveals significant hydrological linkages among different water bodies in the catchment, with particularly well-defined pathways connecting rainfall, pond water, pore water, and fissure water (Fig. 9a, b). Rainfall contributes over 73% to pore water recharge, far exceeding the <17% contribution from pond water (Fig. 9c). However, the SEM results indicate that the direct effect of pond water on pore water is stronger than that of rainfall (Fig. 9b). This apparent contradiction likely stems from the strong statistical association between rainfall and pond water, as pond water is primarily derived from rainfall and shares similar isotopic signatures.

These findings underscore the importance of integrating multiple lines of evidence rather than relying solely on SEM outputs. For example, chloride concentrations in pore water more closely resemble those of pond water, suggesting that pond water may contribute to pore water recharge under specific

删除了: 7

删除了: 5

删除了: site-scale recharge

删除了: 8a

删除了: Several key pathways identified in the model are supported by multiple lines of observational evidence, including isotopic composition, chloride concentrations, and water age (ITTP).

删除了: 8c

删除了:

删除了: total

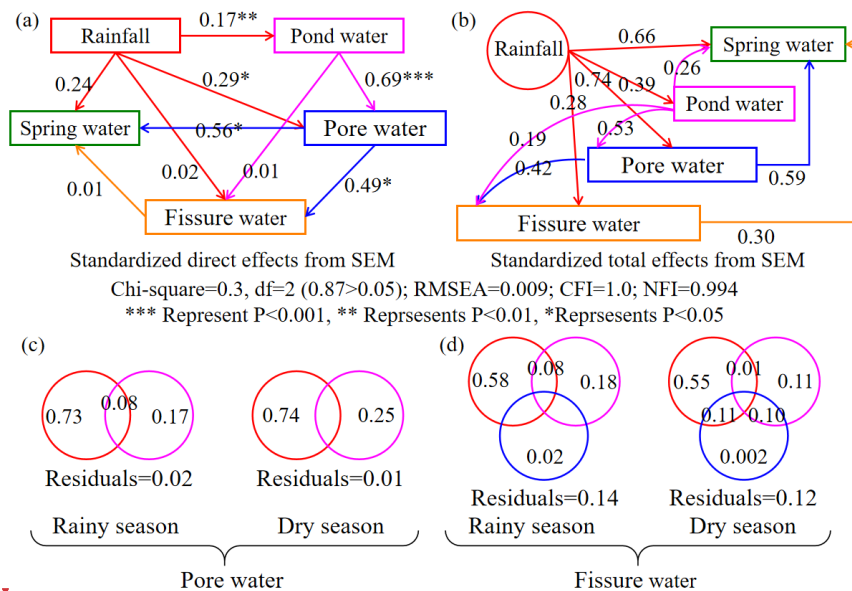
删除了: 8b

删除了: In SEM, the total effect includes both direct pathways (e.g., pond water  $\rightarrow$  pore water) and indirect pathways mediated by other variables (e.g., rainfall  $\rightarrow$  pond water  $\rightarrow$  pore water).

删除了: As a result, the model may overestimate pond water's influence on pore water due to overlapping signals and correlated pathways.

带格式的: 缩进: 首行缩进: 2 字符

791 spatial or temporal conditions (Fig. 7a). The spatial distributions of chloride concentration and  $\delta^{18}\text{O}$   
 792 further show that part of the pore water plots near the precipitation–pond water mixing line, providing  
 793 evidence that pond water can contribute to pore water recharge, particularly in localized areas or during  
 794 discrete recharge events (Fig. 7b). At deeper levels, the linkage between pore water and fissure water is  
 795 supported by their nearly identical isotope values and similar ITTPs, suggesting a shared subsurface  
 796 origin and a strong hydrological connection (Fig. 9a, b). In contrast, although there is some hydrological  
 797 connectivity between pore water and spring water, differences in isotopic slopes and residence times may  
 798 lead to an overestimation of their interaction. However, their nearly identical spatial distributions of  
 799 chloride concentrations and  $\delta^{18}\text{O}$ , provide more direct and reliable evidence of connectivity.



800  
 801 Fig. 9. Structural equation modeling (SEM) and variance partitioning results illustrating hydraulic  
 802 connectivity among water sources in the gully region of the Loess Plateau. Panels (a) and (b) show the  
 803 standardized direct (a) and total effects (b) among rainfall, pond water, pore water, spring water, and  
 804 fissure water, based on  $\delta^{18}\text{O}$  and  $\delta^2\text{H}$  data. In SEM, the total effect includes both direct pathways (a; e.g.,  
 805 rainfall → pore water) and indirect pathways mediated by other variables (b; e.g., rainfall → pond water  
 806 → pore water). Arrows indicate hypothesized water flow pathways, with line thickness proportional to  
 807 effect size. Asterisks denote statistical significance (\*P < 0.05, \*\*P < 0.01, \*\*\*P < 0.001). The model fit  
 808 is excellent ( $\chi^2 = 0.3$ , df = 2, RMSEA = 0.009, CFI = 1.0, NFI = 0.994), supporting the robustness of these

删除了: suggesting mixed recharge from both sources and highlighting the potential for pond water to play a prominent role under certain spatial or temporal conditions (Fig. 2a). Although dry-season isotopic data provide limited support for a strong pond water–pore water connection, the spatial distribution of chloride offers compelling evidence that pond water can contribute significantly to pore water recharge, particularly in localized areas or during specific recharge events.

删除了: 8a

设置了格式: 字体: (默认) Times New Roman

删除了: chloride concentrations

删除了: ...

删除了: 8

824 inferred connections. Panels (c) and (d) present variance partitioning results showing the relative  
825 contributions of source waters to pore water and fissure water during the rainy and dry seasons,  
826 respectively. In panel (c), rainfall (red) and pond water (pink) explain a large portion of pore water  
827 variability, with some shared explanatory power and modest residuals. In panel (d), fissure water reflects  
828 a more complex origin, with contributions from rainfall (red), pond water (pink), and pore water (blue),  
829 and greater overlap and residuals, especially during the dry season.

830

831 Although the model results initially suggest that rainfall, mediated through pond water, is the  
832 primary source of pore water recharge, discrepancies among the different indicators call for a more  
833 critical interpretation of the evidence. The contradictions observed across isotopic, chloride, and ITTP  
834 data underscore the need for further quantitative validation. To address the contradictions observed in the  
835 SEM and variance partitioning results, we apply the water table fluctuation method to independently  
836 estimate the recharge rate from rainfall to pore water. Groundwater level fluctuations in the gully system  
837 revealed clear seasonal recharge dynamics, with an initial rise in the pore water table beginning on  
838 October 24, 2023, followed by a decline through early spring (March 1, 2024) and a gradual recovery  
839 starting June 20, 2024 (Fig. [10a](#)). Between October 24, 2023, and October 24, 2024, cumulative recharge  
840 was estimated at  $238.0 \pm 6.0$  mm (RISE) and  $241.4 \pm 6.0$  mm (MRC), with 159 and 167 recharge days,  
841 respectively (Fig. [10b, c](#)). Given that annual precipitation totaled approximately 550 mm, “site-scale”  
842 recharge was approximately 43–44%, underscoring the significance of focused infiltration in sustaining  
843 shallow aquifer recharge within the gully environment.

844 Site-scale recharge is lower than the precipitation-to-pore water contribution estimated by the  
845 variance decomposition method and may more accurately reflect “actual” recharge, as statistical  
846 estimates can be biased by similarities in isotopic signatures. Combined with dual-isotope and SEM  
847 analyses, the WTF results support a conceptual model where storm runoff is captured and redistributed  
848 through loess soils and retention structures, enabling both shallow and deeper subsurface flow. These  
849 flow paths link pore water, fissure water, and spring discharge across the complex gully landscape,  
850 reflecting both vertical and lateral connectivity within the groundwater system.

带格式的：缩进：首行缩进： 2 字符

删除了：9a

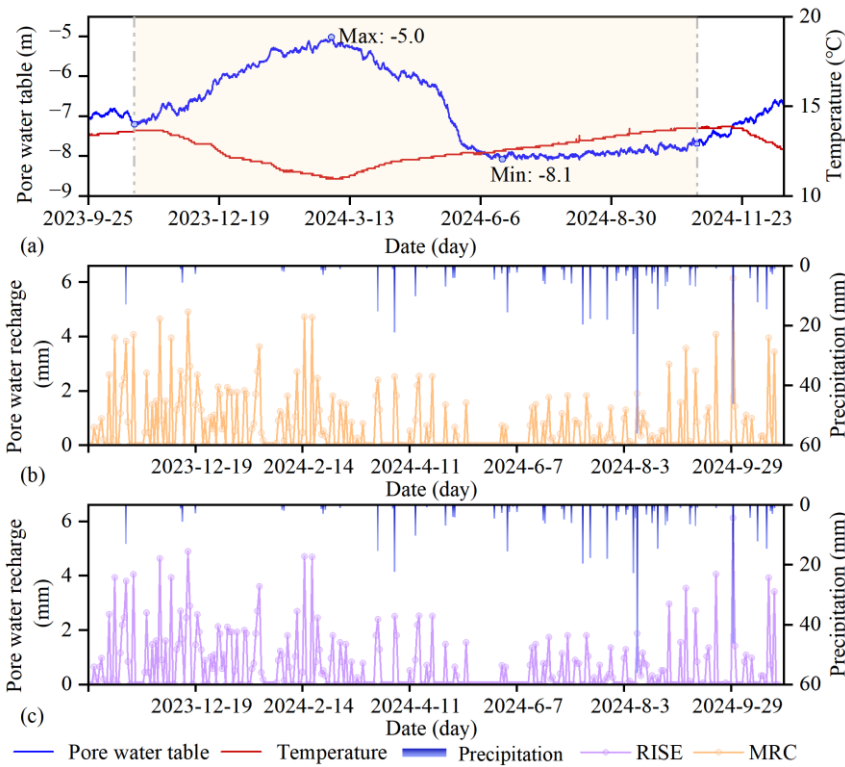
删除了：9b

删除了：recharge efficiency

删除了：This

删除了：efficiency

删除了：When integrated with dual-isotope and SEM analyses, the WTF-based results support a conceptual model in which storm-driven runoff is efficiently captured and redistributed through loess soil matrices and retention structures (e.g., ponds, check dams), activating a hierarchy of shallow and deeper subsurface flowpaths.



862

863

864

865

866

867

868

869

870

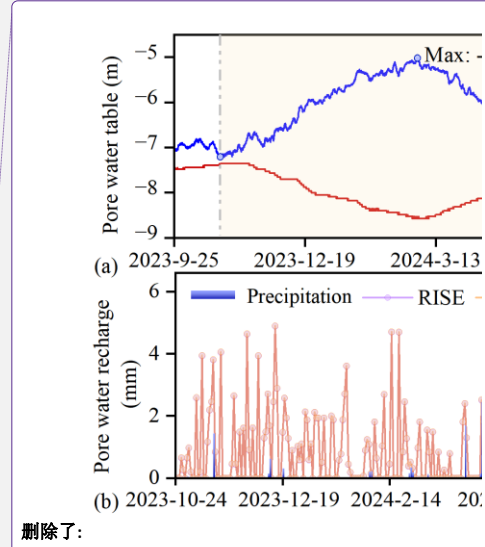
871

872

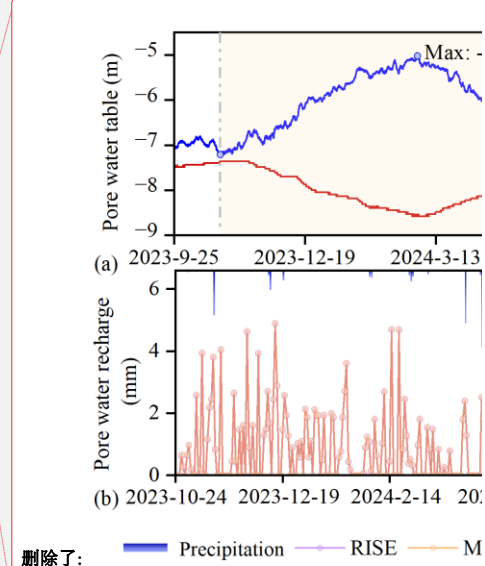
873

874

Fig. 10. Temporal dynamics of pore water table depth, temperature, precipitation, and recharge in the gully region of the Loess Plateau. (a) Daily time series of pore water table depth (blue line) and surface temperature (red line) from September 2023 to November 2024. The water table fluctuates seasonally, rising from  $\sim -8.1$  m in late summer to a maximum of  $\sim -5.0$  m in early spring (March 2024), indicating delayed infiltration and cool-season recharge. (b) Daily precipitation (blue bars) and modeled pore water recharge estimates using the MRC methods. (c) Daily precipitation (blue bars) and modeled pore water recharge estimates using the RISE methods. Most recharge events occur from October to April, even when rainfall is not especially high, while warm-season precipitation contributes little to recharge, likely due to increased evaporative losses and shallow soil retention. Together, these patterns suggest strong seasonal control on recharge processes, with effective infiltration primarily occurring during cooler, low-evaporation periods.



删除了:



删除了:

删除了: 9

删除了: RISE and

删除了: —

880 **5. Discussion**

881 **5.1. Isotopic compositions of various water bodies in the gully region**

882 In hydrological studies, the isotopic composition of water bodies reflects both sources and changes  
883 in hydrological processes (Wan and Liu, 2016; Kumar et al., 2019; Dasgupta et al., 2024). Precipitation,  
884 surface water, and groundwater usually exhibit differences in isotopic characteristics due to variations in  
885 evaporation, infiltration, and mixing (Gleeson et al., 2016; Kuang et al., 2019; Al-Oqaili et al., 2020).  
886 However, similar isotopic distributions among different water bodies often indicate a strong hydrological  
887 connection in their water sources (Yang and Wang, 2023).

888 Our study found that rainfall and pond water have similar spatial isotopic distribution patterns,  
889 indicating that pond water primarily originates from rainfall. This reflects the region's geographical and  
890 hydrological characteristics. In this severely eroded gully region, the local government has constructed  
891 an extensive network of ponds and check dams to capture hillside runoff (Liu et al., 2017; Xue et al.,  
892 2025). As a result, most precipitation from the hills converges into these gully ponds and check dams. A  
893 lower pond water line slope indicates evaporation fractionation during retention. Evaporation  
894 preferentially removes lighter isotopes ( $^1\text{H}$  and  $^{16}\text{O}$ ), enriching heavier isotopes ( $^2\text{H}$  and  $^{18}\text{O}$ ) and shifting  
895 the pond water's isotopic composition from its precipitation source (Aragu et al., 1998; Zhang and Wu,  
896 2009; Gleeson et al., 2016). This similarity is primarily due to the fact that pond water originates from  
897 rainfall and its runoff in the hilly-gully region (Liu et al., 2011; Ji et al., 2024). Additionally, the isotopic  
898 values of most groundwater in the gully areas are more depleted compared to those of rainfall and pond  
899 water, likely due to the recharge mechanisms and residence times of different groundwater types, and the  
900 inherent isotopic characteristics of their primary recharge sources (Ouali et al., 2024). The depleted  
901 signatures in groundwater reflect preferential capture of isotopically light summer monsoon events, with  
902 effective percolation delayed to cooler seasons due to transient soil storage and minimized evaporation,  
903 consistent with observed water table rises predominantly from October to April. Nevertheless, these  
904 values fall within the range of precipitation isotopic values, leaning towards the more negative end. This  
905 suggests two complementary mechanisms: (1) the thin unsaturated zone (<10 meters) provides  
906 preferential pathways for rapid infiltration of precipitation, minimizing evaporative fractionation, and (2)  
907 groundwater is likely recharged primarily by intense precipitation events (e.g., summer storms) with  
908 inherently more negative isotopic signatures (Liu, 2024). Together, these processes explain the observed  
909 isotopic characteristics of groundwater.

删除了: 6

设置了格式: 字体颜色: 自动设置

带格式的: 标题 3

删除了: 6

删除了: —

删除了: Additionally, the isotopic values of most groundwater in the gully areas are more depleted compared to those of rainfall and pond water, likely due to the recharge mechanisms and residence times of the different groundwater types (Ouali et al., 2024). Nevertheless, these values fall within the range of precipitation isotopic values, leaning towards the more negative end, suggesting that groundwater is likely directly recharged by significant precipitation events. This is due to the thin unsaturated zone (<10 m) in the gully areas, which facilitates rapid infiltration and direct recharge from heavy rainfall.

924 To further investigate the complexity of different types of groundwater in the gully area, we  
925 conducted hydrological and geological surveys, collecting water samples from spring water, pore water,  
926 and fissure water. The results show that the isotopic values of spring water, pore water, and fissure water  
927 are closely clustered, indicating a strong interconnection among the different types of groundwater within  
928 the hydrological cycle. This is likely due to their shared geological and hydrological environments  
929 (Bouwer, 2002; Li et al., 2021; Zhang et al., 2022). Our study found that the water line slope of pore  
930 water and fissure water was higher in the dry season than in the rainy season, with values falling between  
931 the slopes of pond water from the rainy and dry seasons. To investigate the cause of these results, we  
932 analyzed groundwater level dynamics, which showed that water tables were lower at the end of the rainy  
933 season but rebounded afterward, making dry-season tables higher. This suggests that rainy-season  
934 groundwater mixes with evaporatively enriched water, lowering its slope, while dry-season groundwater  
935 is recharged by delayed rainfall and pond water, increasing its slope. These findings reveal that isotopic  
936 composition is influenced by both current and prior hydrological conditions. They also highlight the  
937 complexity of evaporation fractionation regulated by water mixing and demonstrate the significant  
938 impact of pond construction on groundwater recharge and regional hydrology in the gully regions.

939

## 940 **5.2. Groundwater recharge processes in the gully region**

941 In recent years, discussions of groundwater recharge sources on the Loess Plateau have largely  
942 focused on tableland and hilly areas characterized by thick loess deposits, whereas gully regions have  
943 received comparatively limited attention (Li et al., 2017; Xiang, 2020; Lu, 2020). For instance, Liu et al.  
944 (2011) demonstrated that groundwater near valley bottoms in hilly loess areas can be replenished by a  
945 combination of precipitation, runoff, and surface water. Our results are broadly consistent with these  
946 earlier findings, but extend them by providing multiple lines of site-specific evidence. Based on stable  
947 isotope signatures and chloride concentrations, we independently identify precipitation and surface water  
948 as the primary sources of groundwater recharge in gully systems. Furthermore, by applying a structural  
949 equation model (SEM), we quantitatively evaluate the relative importance of different recharge pathways,  
950 demonstrating that surface water (particularly pond water) plays a key mediating role in transferring  
951 precipitation inputs to subsurface pore water. Building on these results, we classify groundwater in the  
952 study area into three functional types, spring water, pore water, and fissure water, and propose a  
953 progressive, multi-stage recharge framework: (1) direct recharge of pond water by precipitation and

删除了: 6

955 indirect recharge of pore water by precipitation; (2) focused recharge from pond water to pore water; and  
956 (3) downward percolation from pore water to fissure water. This framework highlights the complexity of  
957 groundwater flow and recharge processes in gully-dominated landscapes and underscores the significant  
958 influence of human interventions, such as ponds and check dams, on modifying hydrological  
959 connectivity and recharge dynamics.

960 In the deep-profile unsaturated zones of the hilly region on the Loess Plateau, previous studies have  
961 used chloride mass balance and tritium peak methods to estimate groundwater recharge from  
962 precipitation, typically accounting for 2%–22% of annual rainfall, with water residence times in the  
963 unsaturated zone lasting several years or even hundreds of years (Huang and Pang, 2011; Tan et al., 2016;  
964 Li et al., 2017; Wang et al., 2024). However, these studies did not address the catchment role of gully  
965 regions. Field observations and past studies show that precipitation rarely directly infiltrates thick loess  
966 in hilly areas (Xu et al., 1993; Li, 2001). Instead, it forms surface runoff that converges into engineered  
967 gullies and accumulates in ponds or other water bodies (perched water), serving as a concentrated  
968 recharge source for groundwater (Yu et al., 2025), reflecting the sustained and delayed impact of gully  
969 runoff on groundwater recharge, which is consistent with the results of this study. In summary, while  
970 hillslope-scale studies describe a “dispersed recharge” mode, where precipitation percolates slowly  
971 through thick unsaturated zones, this study identifies a “concentrated recharge” mode in engineered  
972 gullies, driven by runoff convergence and regulated by check dams via ponding. These fundamentally  
973 distinct modes, differing in hydrological processes, spatial scales, and recharge efficiencies, collectively  
974 enhance the understanding of groundwater recharge mechanisms on the Loess Plateau.

975 Notably, our study does not consider confined water. Tan et al. (2016) indicated that the groundwater  
976 in the high mountain-hilly loess aquifer does not originate from the upwelling of ancient regional  
977 groundwater, and there is no evidence of deep confined water beneath the loess strata in the high  
978 mountain-hills. Additionally, our findings represent only the groundwater recharge results in the gully  
979 regions for two reasons: (1) The hydrological system is complex, with significant variations across  
980 different landscapes of the Loess Plateau (Li et al., 2019; Li et al., 2021). For example, Li et al. (2019)  
981 found that groundwater dominates the hydrological system in the tableland on the Loess Plateau, where  
982 surface water (streams) is recharged by groundwater because river channels are deeper than the bedrock.  
983 (2) Our data collection focused on gully because the “Loess Liang” and “Loess Mao” hillside areas are  
984 covered by thick loess with minimal water sources.

删除了: In recent years, discussions of groundwater recharge sources have primarily focused on tableland and hilly areas with thick loess deposits, although only a few researchers have examined gully regions (Li et al., 2017; Xiang, 2020; Lu, 2020). For example, Liu et al. (2011) found that groundwater near valleys in the hilly loess area is replenished by precipitation, runoff, and surface water. Our findings support this study, identifying rainfall and surface water as major sources of gully groundwater recharge. We classify groundwater into three types (spring water, pore water, and fissure water) and propose a gradual recharge process, including (1) direct and indirect recharge from precipitation to pond water and pore water, respectively; (2) concentrated recharge from pond water to pore water; and (3) percolation recharge from pore water to fissure water. This reflects the complexity of the groundwater system and the significant impact of human activities (e.g., ponds and check dams) on hydrological processes

删除了: et al.

1004  
1005  
1006  
1007  
1008  
1009  
1010  
1011  
1012  
1013  
1014  
1015  
1016  
1017  
1018  
1019  
1020  
1021  
1022  
1023  
1024  
1025  
1026  
1027  
1028  
1029  
1030  
1031  
1032  
1033

### 5.3. Groundwater recharge rates in the gully region

In many parts of the world, identifying the sources of groundwater recharge and its renewability is essential for effective water resource management (Ajjur and Baalousha, 2021; Meles et al., 2024). In the hilly-gully region of the Loess Plateau, where groundwater is considered a crucial source of safe water, understanding the origins and recharge of aquifers provides valuable information for water resource planners (Wang et al., 2006; Liu et al., 2011; Wang et al., 2024). This knowledge is essential and should be shared with regions facing similar challenges.

Groundwater recharge can be quantified from three hydrological sources: surface water, the unsaturated zone, and the saturated zone (Scanlon et al., 2022). Recharge estimates based on the saturated zone are generally more reliable than those from the unsaturated zone, as the latter represents potential recharge that may not ultimately reach the groundwater table (Beven and Germann, 2013; Huang and ~~Shao~~, 2019). The groundwater table fluctuation method is widely used for estimating saturated zone recharge due to its high temporal resolution and intuitive nature (Gumula-Kawęcka et al., 2022; Xu et al., 2024). In our study area, ITTPs estimated similar transit times for both pore water and fissure water. Therefore, we used the groundwater table fluctuation method to assess the recharge of pore water in the gully region. The total recharge from 2023 to 2024 was estimated at  $241.4 \pm 6.0$  mm and  $238 \pm 6.0$  mm using the MRC and RISE methods, respectively. Under constant specific yield conditions, the MRC method typically estimates higher groundwater recharge and recharge days than RISE, as it accounts for groundwater table decline due to lateral outflow and other discharge processes in the absence of recharge (Heppner and Nimmo, 2005). Our findings support this pattern. Furthermore, [the key parameter for estimating groundwater recharge using the water table fluctuation method is specific yield \( \$S\_y\$ \), which depends on soil properties and water table depth \(Liang et al., 2015\). Shallow soil measurements \(0–50 cm\) using the test pit method \(total porosity minus field capacity\) yielded  \$S\_y \approx 0.03\$ , consistent with high capillary retention in near-surface loess \(Wang et al., 2024\). However, for water tables deeper than 2 m \(as in this study, typically 4–10 m\), the test pit method provides a reliable estimate of aquifer-scale drainable porosity \(Nachabe, 2002; Shah and Ross, 2009; Liang et al., 2015\). Accordingly, we adopted  \$S\_y = 0.032\$ , aligned with values of  \$\sim 0.03\$  reported for similar loess-derived unconfined aquifers on the Loess Plateau \(Wang et al., 2023\). Sensitivity analysis indicates that recharge estimates vary by approximately  \$\pm 25\%\$  across the plausible  \$S\_y\$  range \( \$0.032 \pm 0.008\$ \), reflecting uncertainty in effective](#)

删除了: 6

删除了: et al.

删除了: 6

删除了: 6

1038 [drainable porosity within shallow gully aquifers.](#)

1039 Research on groundwater recharge in the Loess Plateau has mainly focused on deep-profile

1040 unsaturated zones in the tableland and hilly areas, with tracer methods estimating recharge between 9 to

1041 100 mm (Huang [and Pang](#), 2011; Li et al., 2017; [Xiang et al.](#), 2019; Lu, 2020; Wang et al., 2024). In

1042 contrast, our study in the gully region indicates recharge of up to 240 mm, much higher than previous

1043 estimates on deep-profile unsaturated zones. This difference reflects several factors: 1) Unsaturated zone

1044 thickness: In the gully region, the unsaturated zone is generally less than 10 m thick, much shallower

1045 than in tableland and hilly areas (mean thickness of 92.2 m), making infiltration easier and promoting

1046 effective recharge. 2) Gully topography and hydrology, characterized by well-developed channels,

1047 concentrated runoff, and widespread ponds and check dams, promote focused infiltration (Liu et al., 2017;

1048 Li et al., 2021; Xue et al., 2025). 3) Research methods: Tracer methods reflect long-term recharge rates

1049 and are better suited for thicker unsaturated zones (Huang [and Pang](#), 2011; Lu, 2020; Li et al., 2017). In

1050 contrast, the water table fluctuation method directly captures short-term recharge dynamics and works

1051 better in thinner unsaturated zones. Moreover, this method also better captures surface water-

1052 groundwater interactions and focused recharge effects (Gumuła-Kawęcka et al., 2022). These findings

1053 underscore the importance of studying recharge in gully regions, filling a research gap in the Loess

1054 Plateau's geomorphology and providing new ecohydrological insights. [However, the robustness of our](#)

1055 [findings requires further exploration. On one hand, due to the limited spatial distribution of sampling](#)

1056 [points, the current results primarily reflect the hydrological characteristics of engineered gullies, and](#)

1057 [their representativeness at the regional scale requires validation through future expansion of the](#)

1058 [monitoring network. On the other hand, the study period did not encompass extreme precipitation or](#)

1059 [drought events, which may significantly alter surface flow convergence conditions and vadose zone](#)

1060 [water transport mechanisms, thereby substantially impacting recharge processes. Future work should](#)

1061 [strengthen dynamic monitoring and simulation analysis under extreme hydrological scenarios.](#)

#### 1063 5.4. Revised conceptual model

1064 To convey our evolving understanding of the spatial structure and dynamics in the Gully Region,

1065 we developed a conceptual model that [traces precipitation's transformation into subsurface water, from](#)

1066 [runoff capture and surface ponding in dammed gully reaches, through infiltration in the unsaturated zone,](#)

1067 [to recharge in both shallow, porous aquifer and deeper bedrock fissure systems](#) (Figure 11). This

删除了: Uncertainty analysis showed that recharge estimates vary by  $\pm 25\%$  for  $S_y$ , which ranges from  $3.2 \pm 0.8\%$ .

删除了: the key parameter for estimating groundwater recharge using the groundwater table fluctuation method is specific yield, which depends on factors such as soil properties and water table depth. This value can be derived from empirical soil texture, pumping tests, or the test pit method (Nachabe, 2002; Liang et al., 2016). Shah and Ross (2009) found the test pit method reliable for water tables deeper than 2 m. In this study, with a water table exceeding 2 m, the specific yield was 0.32, consistent with values of 0.3 in similar soil conditions (Wang et al., 2023).

删除了: et al.

删除了: —

删除了: —

删除了: —

删除了: —

删除了: et al.

删除了: localized typical

删除了: Furthermore, our study demonstrates the potential of artificial ponds to regulate water resources and enhance recharge, with valuable implications for water management and ecological engineering.

删除了: 6

删除了: gullies

删除了: the

删除了:

删除了: Through this integrative framework, we elucidate the transformation of precipitation into various forms of subsurface water by explicitly tracing its movement through a cascade of compartments—from surface ponding in dammed gullies, to infiltration through the unsaturated zone, and eventual recharge into both the porous aquifer and underlying bedrock fissure systems....

1102 conceptual reframing is grounded in the stark contrasts between hydrological processes active on hilly  
 1103 uplands and managed gully systems. In the hilly uplands, ~~previous studies have shown that~~ thick loess  
 1104 deposits, ~~often exceeding 90 m (including low-permeability aquifers), combined with steep slopes (>15°)~~  
 1105 severely restrict vertical infiltration (~~Zhu et al., 2018; Huang et al., 2019; Huang et al., 2024~~).  
 1106 Compounded by short-duration, high-intensity rainfall events that provide insufficient moisture for deep  
 1107 profile wetting, rainfall is converted rapidly into surface runoff (Li et al., 2021). ~~Our new work shows~~  
 1108 that, ~~runoff is systematically funneled downslope into gully systems, as a consequence of ecological~~  
 1109 ~~engineered~~ check dams and retention ponds that intercept and concentrate overland flow. ~~Most~~  
 1110 infiltration occurs after surface water accumulates in fill zones of ~~engineered~~ gullies. Ponds and perched  
 1111 water bodies subsequently serve as ~~localized recharge foci~~.  
 1112 Crucially, gully systems possess distinct hydrogeological characteristics: the loess mantle is much  
 1113 thinner (typically < 25 m), and the soils are dominated by silt loam textures with moderate specific yield  
 1114 (0.02–0.05) and high field capacity (21–28%). These properties promote transient water storage and  
 1115 enable temporally delayed ~~and~~ depth-partitioned infiltration. Based on our integrated analyses of stable  
 1116 isotopes, chloride concentrations, and inverse transit time proxies, we find that ~~engineered gullies~~  
 1117 ~~function not as passive erosional features but as active, managed recharge conduits~~. This  
 1118 conceptualization captures a critical spatial transition, ~~from runoff generation in the hilly uplands to~~  
 1119 ~~focused recharge in gully zones, emphasizing the pivotal role of gully systems in regulating groundwater~~  
 1120 ~~recharge across the Loess Plateau landscape~~.  
 1121 Combined hydrological monitoring and multi-indicator analysis further reveal that following the  
 1122 rainy season, infiltration depths on hilly slopes are typically shallow, ~~(less than 1 m), while groundwater~~  
 1123 levels in gully areas exhibit pronounced rises exceeding 2 m (~~Fig. 11~~). Recharge estimates based on the  
 1124 water table fluctuations reach up to ~~approximately~~ 240 mm ~~at the monitored gully reach~~, far surpassing  
 1125 values observed in deep unsaturated zones of tablelands and hills (Huang ~~and Pang~~, 2011; Li et al., 2017;  
 1126 Lu, 2020; Wang et al., 2024). ~~The results of this study reinforce the role of engineered gully reaches as~~  
 1127 ~~focal points for groundwater recharge and further quantify site-scale pore-water recharge equivalent to~~  
 1128 ~~~43% of mean annual precipitation, a finding that highlights the efficiency of focused infiltration under~~  
 1129 ~~managed conditions~~. This value reflects spatially focused recharge under conditions of runoff  
 1130 convergence and ponding, and should not be interpreted as representative of hillslope or catchment-wide  
 1131 recharge rates.

- 删除了:—
- 删除了:—
- 删除了:; Zhu et al., 2018
- 设置了格式: 字体: (默认) Times New Roman, 10 磅, 字体颜色: 文字 1
- 删除了: This
- 删除了: , a process further intensified
- 删除了: . Because precipitation seldom infiltrates directly into the thick loess of upland regions (Xu et al., 1993; Li, 2001), m
- 删除了:—
- 删除了: focal points for groundwater recharge
- 删除了: (Yu et al., 2025).
- 删除了: ,
- 删除了: gullies function not as passive erosional features but as active recharge conduits.
- 删除了:—
- 删除了:—
- 删除了:—
- 删除了: et al.
- 删除了:
- 删除了: ies
- 删除了:
- 删除了: the recharge rate of pore water at 43%, a crucial finding for understanding groundwater recharge mechanisms in semi-arid regions.
- 删除了: These results reinforce the role of gullies as focal points for groundwater recharge and are consistent with prior studies. For instance, in hilly areas, precipitation rarely recharges groundwater due to the thick loess layers, with an average infiltration depth of only 1 meter (Wang et al., 2024).

1162 Liu et al. (2011) found that groundwater near valleys in the hilly loess area is replenished by  
1163 precipitation, runoff, and surface water. Moreover, fissure water exhibits more depleted isotopic  
1164 signatures and higher chloride concentrations, indicating deeper percolation of pore water or mixing with  
1165 older recharge sources (Fig. 11). These patterns, supported by ITTPs and statistical (SEM-based)  
1166 connectivity indicators, reveal a hierarchical recharge sequence: event-driven infiltration enters a porous  
1167 shallow aquifer, some of which slowly percolates into deeper fissure zones. This hierarchical mechanism  
1168 is facilitated by the combination of thin loess mantles, engineered interventions (e.g., check dams and  
1169 ponds), and delayed hydrological responses.

删除了: partial SEM linkages

删除了: the shallow pore

1170 By integrating multiple lines of evidence, this conceptual model redefines engineered gullies as  
1171 selective recharge corridors whose hydrological function emerges from the interaction between  
1172 geomorphic structure and human intervention. It challenges the traditional view of gullies as purely  
1173 erosional landforms and emphasizes their dual hydrological function: acting both as runoff conveyance  
1174 channels and as transient reservoirs that store and redistribute water across space and time. This recharge  
1175 capacity is jointly governed by topographic convergence, reduced loess thickness, and the presence of  
1176 engineered structures such as check dams and retention ponds that increase residence time.

删除了: shaped by both

1177 Crucially, the model offers insight into the multifunctionality of ecological engineering, particularly  
1178 check dams and ponds in enhancing groundwater recharge, and supporting ecosystem restoration across  
1179 the Loess Plateau. This study proposes a cascade-type recharge framework for engineered gully systems,  
1180 highlighting the role of engineered gullies as convergence pathways that locally focus infiltration and  
1181 groundwater recharge. Rather than invoking preferential flow within the soil matrix, this framework  
1182 emphasizes topographic convergence, stratigraphic thinning, and engineered ponding as the dominant  
1183 mechanisms that promote spatially concentrated recharge within gully zones. While this process is  
1184 demonstrated using site-specific tracer and water-table observations, its broader relevance at the  
1185 catchment scale remains conceptual and warrants further investigation. Furthermore, water movement  
1186 within the silted loess layer of the gully system remains dominated by a piston flow pattern (Yu et al.,  
1187 2025). By identifying the pivotal role of gully systems in stormwater detention, delayed infiltration, and  
1188 depth-partitioned recharge, this study establishes a mechanistically grounded conceptual basis improving  
1189 water resource allocation, infrastructure planning, and groundwater sustainability in arid and semi-arid  
1190 regions.

删除了: .

删除了: —

删除了: —

删除了: hydrological regulation, water security, and ecosystem restoration

删除了: This study identifies a distinctive cascade-type recharge process in loess gully catchments and proposes the “gully-dominated preferential recharge mechanism”. This mechanism emphasizes the hydrological function of gullies as convergence pathways and efficient recharge windows at the catchment scale, rather than preferential flow paths within the soil matrix.

删除了: Compared to the traditional piston-flow and preferential flow models commonly applied in the region, the proposed “gully-dominated preferential recharge mechanism” marks a notable theoretical advancement. Whereas previous models primarily emphasize vertical infiltration through homogeneous loess layers, this study is the first to quantitatively identify a cascade recharge process unique to thin-loess gully catchments.

删除了: multi-aquifer

删除了: robust theoretical and technical foundation for

1191 However, with the reconstruction of gully systems and ecological restoration, attention must also

1217 be given to the potential risks of pollutant migration (Yu et al., 2020). The hydrological functions of  
1218 gullies may enhance the movement of pollutants into groundwater, especially in areas with intensive  
1219 human activities, where pollutants can enter **engineered** gullies through surface runoff and subsequently  
1220 infiltrate the groundwater system. During ecological restoration, excessive human intervention or soil  
1221 improvement measures may lead to the accumulation and dispersion of pollutants, which may  
1222 compromise groundwater security (Liu et al., 2017). Therefore, the protection and rational reconstruction  
1223 of gully systems should not only focus on their hydrological functions but also consider potential  
1224 environmental risks, particularly the pathways of pollutant migration. These findings therefore  
1225 underscore the need to evaluate gully-based restoration strategies within an integrated water-quality and  
1226 groundwater-protection framework (Obuobie et al., 2012; Zhao et al., 2019; Zhao and Wang, 2021; Xue  
1227 et al., 2025).

1228 The study demonstrates how **hydrologically arrested gully systems** can function as critical “recharge  
1229 windows” for groundwater in arid areas. This underscores the importance of **strategically identifying and**  
1230 **managing** gully networks in watershed management, while avoiding excessive filling or hardening to  
1231 preserve their hydrological functions. In ecological restoration projects, directing surface runoff toward  
1232 **engineered gullies under controlled conditions** can efficiently convert limited precipitation into  
1233 groundwater storage, thereby enhancing regional water retention capacity. Beyond advancing theoretical  
1234 understanding of regional hydrological processes, **this conceptual model** provides **a process-based**  
1235 **foundation** for developing spatially targeted models of groundwater recharge **in managed dryland**  
1236 **landscapes**.

删除了: More importantly, these findings have direct implications for land management practices and ecological restoration strategies in similar arid regions worldwide.

删除了: gullies serve

删除了: systematically

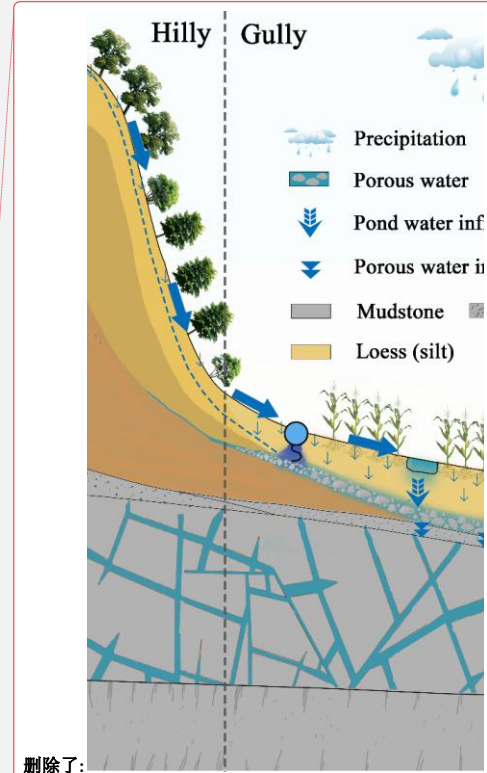
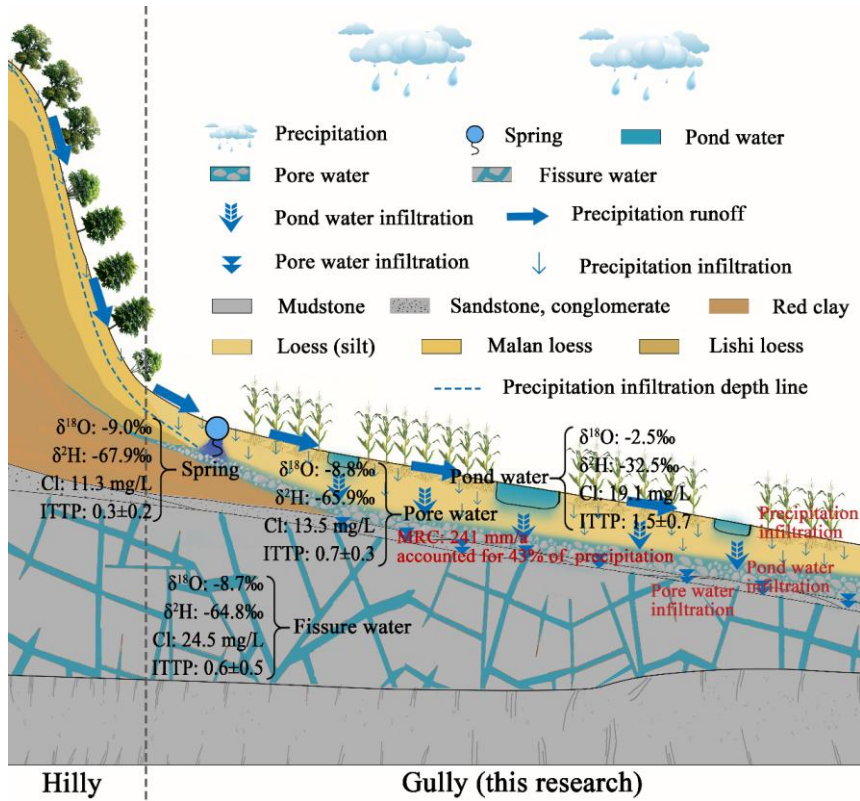
删除了: conserving

删除了: natural

删除了: it also

删除了: a sound basis

删除了: .



删除了:

删除了: 10

删除了: 6

1247  
 1248 Fig. 11. Hydraulic connections between different water bodies in the hilly-gully region of the Loess  
 1249 Plateau. The study area consists of hilly and gully regions. In the hilly area, the stratigraphic sequence  
 1250 from top to bottom is Malan loess, Lishi loess, red clay, sandstone, and mudstone. Rainfall infiltration  
 1251 within the Malan loess is less than 1 m, and the area is mainly covered by vegetation. In the gully area,  
 1252 the stratigraphy from top to bottom includes loess (silt), sandstone and conglomerate, and mudstone.  
 1253 Pore water is found within the sandstone and conglomerate, while fissure water occurs in bedrock  
 1254 fractures (mudstone). Numerous check dams or ponds are distributed throughout the gully area. The  
 1255 vertical separation between the pore water and pond water ranges from 3 to 5 m. Corn is the main crop  
 1256 cultivated in this region. Most springs in the study area are located at the junction of the hilly and gully  
 1257 regions and are discharged from pore water.

1258

1259 **5.5. Limitations and future research directions**

1260 This study underscores the limitations of relying on a single indicator to infer localized groundwater

1264 recharge pathways, as doing so may lead to oversimplified or potentially misleading interpretations of  
1265 complex hydrological processes. While stable isotope signatures suggest precipitation contributes to pore  
1266 aquifer recharge, they do not provide clear evidence of direct recharge from pond water to either pore or  
1267 fissure groundwater during the dry season. In contrast, the spatial distribution of chloride concentrations  
1268 offers compelling support for focused pond water leakage into the shallow groundwater system.

1269 Without explicit mass-balance constraints, structural equation modeling may not independently or  
1270 quantitatively represent actual groundwater flow processes. In contrast, the water-table fluctuation  
1271 method, which directly measures changes in groundwater levels, provides a more empirically grounded  
1272 estimate of total recharge. Each approach nevertheless offers distinct strengths: water-table fluctuations  
1273 resolve the timing and magnitude of recharge, whereas isotopic, hydrochemical, and modeling analyses  
1274 yield critical insights into recharge sources and flow pathways. By leveraging the complementarity and  
1275 mutual corroboration of these methods, our study robustly demonstrates the pivotal role of gully areas in  
1276 groundwater recharge.

1277 Despite effort to address uncertainties, limitations remain in terms of spatial and temporal sampling  
1278 density. For example, the lack of long-term tracers such as groundwater age, combined with limited  
1279 observations of groundwater level fluctuations, constrains our ability to assess recharge dynamics over  
1280 multi-year timescales. Additionally, the current sampling design includes only two campaigns during the  
1281 rainy and dry seasons, which may be insufficient to fully capture the seasonal variability of ITTP values.  
1282 This, in turn, may affect the accuracy of groundwater renewal frequency estimates and the strength of  
1283 inferred hydrological connections. In arid and semi-arid regions, groundwater recharge is typically  
1284 triggered by infrequent, high-intensity rainfall events. However, existing sampling strategies based on  
1285 seasonal intervals often lack the temporal resolution necessary to capture these short-lived, event-driven  
1286 recharge processes effectively.

1287 Future research should address these issues through several improvements: (1) conducting higher-  
1288 frequency, event-scale sampling to systematically monitor rainfall, spring discharge, and pond water  
1289 level dynamics, thus capturing the influence of key hydrological events on recharge processes; (2)  
1290 expanding the spatial coverage of pore and fissure well monitoring to improve the accuracy of regional  
1291 recharge pattern identification; and (3) incorporating additional environmental tracers (e.g.,  $^3\text{H}$ ,  $^{22}\text{Na}$ ) to  
1292 trace flow paths and estimate recharge lag times. In addition, systematic observation of event-scale  
1293 hydrological processes should be strengthened by establishing a high-frequency, event-driven monitoring

删除了: regional

删除了: Although variance decomposition analysis and structural equation modeling suggest statistical linkages among different water bodies and provide useful clues about potential recharge pathways, these associations may be confounded by overlapping isotopic signatures or by non-conservative processes such as evaporation and mixing, potentially leading to an overestimation of hydrological connectivity. In the absence of mass balance constraints, the pathways inferred through SEM may not accurately reflect the actual flow processes within the groundwater system. By contrast, the water table fluctuation method captures both vertical and lateral recharge processes, yielding estimates that are more likely to reflect actual recharge rates. Drawing on this empirical evidence, the present study further substantiates the critical role of gully zones in regional groundwater recharge....

1311 network to better capture the nonlinear coupling among rainfall, surface runoff, and groundwater  
1312 dynamics. This approach would significantly improve our understanding of rapid infiltration events and  
1313 associated recharge mechanisms.

1314 From a methodological perspective, integrating statistical techniques, such as SEM and variance  
1315 decomposition analysis, with process-based physical models like MODFLOW and HYDRUS can  
1316 provide mechanistically constrained insights into recharge pathways. Compared to correlation-based  
1317 statistical methods, physical models offer greater precision in characterizing groundwater flow and  
1318 recharge processes across both temporal and spatial dimensions, helping to reduce uncertainties  
1319 associated with non-conservative tracer behavior and the absence of mass balance constraints. Regarding  
1320 measurements, hydrometric instrumentation within check dams and beneath pond beds could further  
1321 quantify the recharge effects of various engineering interventions under specific hydrological conditions.  
1322 Additionally, integrating isotopic data with mean transit time modeling, combined with targeted  
1323 catchment-wide field monitoring and improved spatial analysis, could help elucidate recharge pathways,  
1324 quantify temporal dynamics, and enhance process-level understanding of groundwater recharge  
1325 throughout the catchment of such complex dryland landscapes. Collectively, these efforts will contribute  
1326 to a stronger theoretical foundation and offer practical guidance for the precise management of water  
1327 resources, the design of ecologically appropriate engineering interventions, and the implementation of  
1328 effective landscape rehabilitation strategies.

1329

## 1330 **6. Conclusion**

1331 Through integrated analysis of stable isotopes, chloride concentrations, water-table fluctuations, and  
1332 inverse transit time proxies, this study provides multiple, convergent lines of evidence that engineered  
1333 gully reaches on the Loess Plateau function as hydrologically significant recharge zones, rather than  
1334 solely as products of accelerated erosion and degradation. Precipitation-driven runoff supports  
1335 substantial recharge to shallow pore aquifers, with site-scale recharge magnitudes equivalent to  
1336 approximately 43% of mean annual precipitation at the monitored gully reach. Although evaporative  
1337 fractionation limits the ability of stable isotopes alone to resolve direct recharge from ponded surface  
1338 water, chloride concentrations provide independent evidence consistent with mixing between pond water  
1339 and pore water, complementing the isotopic patterns. Together, these indicators indicate likely hydraulic

删除了:—

删除了:—

删除了: in

删除了: c

删除了: 7

设置了格式: 字体: 非加粗

设置了格式: 字体: 非加粗

1345 connectivity, while not constituting a mass-balanced quantification of recharge sources. Recharge within  
1346 shallow gully-zone aquifers is spatially concentrated and temporally selective, governed by topographic  
1347 convergence, loess stratigraphy, and ecological engineering structures, particularly check dams and  
1348 ponds, which increase surface-water residence time and promote focused infiltration.

1349 These findings offer a process-based framework for developing hydrological indicators of  
1350 landscape function and restoration performance managed in dryland environments. Specifically, recharge  
1351 magnitude, isotopic damping, and solute accumulation patterns may serve as diagnostic indicators for  
1352 identifying effective recharge zones and tracking hydrological response to intervention. To refine these  
1353 indicators, future studies should incorporate high-frequency monitoring, event-based sampling, and  
1354 multi-tracer approaches. Collectively, this work challenges conventional views of gullies as hydrological  
1355 liabilities and demonstrates context-dependent role as targeted recharge assets in engineered dryland  
1356 systems, refining conceptual understanding of dryland groundwater recharge and informing the  
1357 evaluation and design of ecological engineering strategies in similar semi-arid landscapes.

1358  
1359  
1360

1361 **Author contributions:**

1362 ZXJ: Conceptualization, Methodology, Formal analysis, Investigation, Visualization, Data curation,  
1363 Validation, Writing-original draft. ADZ: Conceptualization, Formal analysis, Validation, Visualization,  
1364 Writing-review & editing. LW: Conceptualization, Funding acquisition, Project administration,  
1365 Resources, Supervision, Visualization, Writing-review & editing.

1366 **Data availability:**

1367 All datasets are available at Zenodo: <https://zenodo.org/records/18596600>.

1368 **Conflicts of Interest:**

1369 The contact author has declared that none of the authors has any competing interests.

1370 **Acknowledgments:**

1371 This work was supported by the National Natural Science Foundation of China (grant numbers 42377318  
1372 and U24A20629).

1373

删除了:—

删除了:—that

删除了: Through integrated analysis of stable isotopes, chloride concentrations, water table fluctuations, and inverse transit time proxies, we developed multiple lines of evidence to reframe gullies in the Loess Plateau as hydrologically significant recharge zones, rather than solely as indicators of erosion and degradation. Precipitation events drive substantial recharge to shallow pore aquifers, with annual rates exceeding 238 mm<sup>43</sup>—, accounting for a large fraction of annual rainfall. While isotopic evidence for recharge from pond water is obscured by evaporative fractionation, chloride concentrations, stable isotopes, and SEM provide a clear signal of subsurface connectivity. Recharge in this system is both spatially concentrated and temporally selective, shaped by terrain configuration, loess stratigraphy, and ecological engineering structures such as check dams and ponds.

删除了: foundation

删除了: tools

删除了: system responses

删除了: their underappreciated role as targeted recharge assets—, advancing dryland groundwater sustainability and providing actionable insights for landscape-scale ecological restoration and management.

删除了: Data are available from the corresponding author upon reasonable request.

1400 **References**

1401 Ajjur, S.B., Baalousha, H.M. A review on implementing managed aquifer recharge in the Middle East  
1402 and North Africa region: methods, progress and challenges. *Water International*. 46(4): 578-604, 2021.

1403 [DOI: 10.1080/02508060.2021.1889192](https://doi.org/10.1080/02508060.2021.1889192).

删除了: <https://doi.org/>

1404 Al-Oqaili, F., Good, S.P., Peters, R.T., Finkenbiner, C., Sarwar, A. Using stable water isotopes to assess  
1405 the influence of irrigation structural configurations on evaporation losses in semiarid agricultural systems.

1406 *Agricultural and Forest Meteorology*. 291: 108083, 2020. [DOI: 10.1016/j.agrformet.2020.108083](https://doi.org/10.1016/j.agrformet.2020.108083).

删除了: <https://doi.org/>

1407 Aragu, L., Froehlich, K., Rozanski, K. Stable isotope composition of precipitation over southeast Asia.

1408 *Journal of Geophysical Research*. 103(28): 721-728, 1998. [DOI: 10.1029/98JD02582](https://doi.org/10.1029/98JD02582).

删除了: <https://doi.org/>

1409 Berg, A., Findell, K., Lintner, B., Giannini, A., Seneviratne, S.I., Hurk, B.V.D., Lorenz, R., Pitman, A.,  
1410 Hagemann, S., Meier, A. Land-atmosphere feedbacks amplify aridity increase over land under global

1411 warming. *Nature Climate Change*. 6(9): 869-874, 2016. [DOI: 10.1038/nclimate3029](https://doi.org/10.1038/nclimate3029).

删除了: <https://doi.org/>

1412 Beven, K., Germann, P. Macropores and water flow in soils revisited. *Water Resources Research*. 49(6):

1413 3071-3092, 2013. [DOI: 10.1002/wrcr.20156](https://doi.org/10.1002/wrcr.20156).

删除了: <https://doi.org/>

1414 Bouwer, H. Artificial recharge of groundwater: hydrogeology and engineering. *Hydrogeology Journal*.

1415 10(1): 121-142, 2002. [DOI: 10.1007/s10040-001-0182-4](https://doi.org/10.1007/s10040-001-0182-4).

删除了: <https://doi.org/>

1416 Cai, H.E., Zhang, J.W., Zheng, J.G., Zhang, R.S., Liang, X.L. Hydrogeology features of Loess hilly gully  
1417 region in Yan'an. *Geotechnical Engineering Technique*. 33(5): 288-292, 2019. [DOI: 10.3969/j.issn.1007-2993.2019.05.009](https://doi.org/10.3969/j.issn.1007-2993.2019.05.009).

删除了: <https://doi.org/>

1419 Dane, J.H., Topp, C.G., Gee, G.W. 2.4 Particle-Size Analysis. 5: 255-293, 2002.

删除了: Chen, P.Y., Ma, J.Z., Ma, X.Y., Yu, Q., Cui, X.K., Guo, J.B. Groundwater recharge in typical geomorphic landscapes and different land use types on the loess plateau, China. *Hydrological Processes*. 37(4): 14860, 2023. [https://doi.org/DOI: 10.1002/hyp.14860](https://doi.org/10.1002/hyp.14860).

1420 Dasgupta, B., Prakash, P., Sen, R., Noble, J., Chatterjee, S., Sanyal, P. The isotopic composition of the

1421 world's highest river basins: Role of hydrological mixing ratios and transit time. *Journal of Hydrology*.

1422 638: 131544, 2024. [DOI: 10.1016/j.jhydrol.2024.131544](https://doi.org/10.1016/j.jhydrol.2024.131544).

删除了: '

1423 Fu, B.J., Chen, L., Ma, K. The effect of land use change on the regional environment in the Yangjuangou  
1424 catchment in the loess plateau of China. *Acta Geographica Sinica*. 54: 241-246, 1999. [DOI: 10.3321/j.issn:0375-5444.1999.03.006](https://doi.org/10.3321/j.issn:0375-5444.1999.03.006).

删除了: <https://doi.org/>

1425 Fu, B.J., Liu, Y., Lü, Y.H., He, C.S., Zeng, Y., Wu, B.F. Assessing the soil erosion control service of

1426 ecosystems change in the Loess Plateau of China. *Ecological Complexity*. 8 (4): 284-293, 2011. [DOI: 10.1016/j.ecocom.2011.07.003](https://doi.org/10.1016/j.ecocom.2011.07.003).

1427 10.1016/j.ecocom.2011.07.003.

删除了: Feng, X.M., Fu, B.J., Piao, S.L., Wang, S., Ciais, P., Zeng, Z.Z., Lü, Y.H., Zeng, Y., Li, Y., Jiang, X.H., Wu, B.F. Revegetation in China's Loess Plateau is approaching sustainable water resource limits. *Nature Climate Change*. 6: 1019-1022, 2016. [https://doi.org/DOI: 10.1038/nclimate3092](https://doi.org/10.1038/nclimate3092).

1428 10.1016/j.ecocom.2011.07.003.

删除了: <https://doi.org/>

1429 Fu, B.J., Wang, S., Liu, Y., Liu, J., Liang, W., Miao, C. Hydrogeomorphic ecosystem responses to natural

删除了: <https://doi.org/>

1452 and anthropogenic changes in the Loess Plateau of China. Annual Review of Earth and Planetary  
1453 Sciences. 45: 223-243, 2017. DOI: 10.1146/annurev-earth-063016-020552.

1454 Gates, J.B., Scanlon. B.R., Mu. X.M, Zhang, L. Impacts of soil conservation on groundwater recharge in  
1455 the semi-arid Loess Plateau, China. Hydrogeology Journal. 19(4): 865-875, 2011. DOI: 10.1007/s10040-  
1456 011-0716-3.

1457 Gleeson, T., Befus, K.M., Jasechko, S., Luijendijk, E., Cardenas, M.B. The global volume and  
1458 distribution of modern groundwater. Nature Geoscience. 9(2): 161-167, 2016. DOI: 10.1038/NCEO2590.

1459 Gumuła-Kawęcka, A., Jaworska-Szulc B., Szymkiewicz A., Gorczewska-Langner W., Pruszkowska-  
1460 Caceres M., Angulo-Jaramillo R., Šimůnek J. Estimation of groundwater recharge in a shallow sandy  
1461 aquifer using unsaturated zone modeling and water table fluctuation method. Journal of Hydrology. 605:  
1462 127283, 2022. DOI: 10.1016/j.jhydrol.2021.127283.

1463 He, M.N., Wang, Y.Q., Tong, Y.P., Zhao, Y.L., Qiang, X.K., Song, Y.G., Wang, L., Song, Y., Wang, G.D.,  
1464 He, C.X. Evaluation of the environmental effects of intensive land consolidation: A field-based case  
1465 study of the Chinese Loess Plateau. Land Use Policy. 94: 104523, 2020. DOI:  
1466 10.1016/j.landusepol.2020.104523.

1467 Healy, R.W., Cook, P.G. Using groundwater levels to estimate recharge. Hydrogeology Journal. 10(1):  
1468 91-109, 2002. DOI: 10.1007/s10040-001-0178-0.

1469 Heppner, C.S., Nimmo, J.R. A computer program for predicting recharge with a master recession curve.  
1470 U.S. Geological Survey Scientific Investigations Report. 2005-5172, 2005. DOI: 10.3133/sir20055172.

1471 Huang, J., Li, Y., Fu, C., Chen, F., Fu, Q., Dai, A., Wang, G. Dryland climate change: Recent progress  
1472 and challenges. Reviews of Geophysics. 55(3): 719-778, 2017. DOI: 10.1002/2016RG000550.

1473 [Huang L.M., Shao M.A. Advances and perspectives on soil water research in China's Loess Plateau.](#)  
1474 [Earth-Science Reviews. 199\(2\): 102962, 2019. DOI: 10.1016/j.earscirev.2019.102962.](#)

1475 [Huang, L.M., Wang, Z.W., Pei, Y.W., Zhu, X.C., Jia, X.X., Shao, M.A. Adaptive water use strategies of](#)  
1476 [artificially revegetated plants in a water-limited desert: A case study from the Mu Us Sandy Land. Journal](#)  
1477 [of Hydrology, 644: 132103, 2024. DOI: 10.1016/j.jhydrol.2024.132103.](#)

1478 Huang, T.M., Pang, Z.H. Estimating groundwater recharge following land-use change using chloride  
1479 mass balance of soil profiles: a case study at Guyuan and Xifeng in the Loess Plateau of China.  
1480 Hydrogeology Journal. 19: 177-186, 2011. DOI: 10.1007/s10040-010-0643-8.

1481 Huang, T.M., Pang, Z.H., Edmunds, W.M. Soil profile evolution following land-use change: Implications

删除了: <https://doi.org/>

删除了: <https://doi.org/>

删除了: Gee, G. W., Hillel, D. Groundwater recharge in arid regions: Review and critique of estimation methods. Hydrological Processes. 2(3): 255-266, 1988. <https://doi.org/DOI: 10.1002/hyp.3360020306>.

删除了: <https://doi.org/>

1489 for groundwater quantity and quality. *Hydrological Processes*. 27(8): 1238-1252, 2013. DOI:  
1490 10.1002/hyp.9302.

1491 Huang, Y.N., Evaristo, J., Li, Z. Multiple tracers reveal different groundwater recharge mechanisms in  
1492 deep loess deposits. *Geoderma*. 353: 207-212, 2019. DOI: 10.1016/j.geoderma.2019.06.041.

1493 Jasechko, S., Perrone, D. Global groundwater wells at risk of running dry. *Science*. 372(6540): 418-421,  
1494 2021. DOI: 10.1126/science.abc2755.

1495 Ji, M.Y., Jia, D.B., Hao, Y.S., Liu, T., Yang, L.N., Li X.Y., Lv, C.G., Shang Z.Q. Hydrochemical and  
1496 isotopic characteristics and water transformation relationships in the Zhenglan Banner section of  
1497 Shandian River Basin. *Chinese Journal of Applied Ecology*. 1-11, 2024. DOI: 10.13287/j.1001-  
1498 9332.202410.015.

1499 Jia, X.X., Zhu, P., Wei, X.R., Zhu, Y.J., Huang, M.B., Hu, W., Wang, Y.Q., Turkeltaub, T., Binley, A.,  
1500 Horton, R., Shao, M.A. Bringing ancient loess critical zones into a new era of sustainable development  
1501 goals. *Earth-Science Reviews*. 255: 104852, 2024. DOI: 10.1016/j.earscirev.2024.104852.

1502 Jin, Z., Guo, L., Wang, Y.Q., Yu, X.L., Lin, H., Chen, Y.P., Chu, G.C., Zhang, J., Zhang, N.P. Valley  
1503 reshaping and damming induce water table rise and soil salinization on the Chinese Loess Plateau.  
1504 *Geoderma*. 339: 115-125, 2019. DOI: 10.1016/j.geoderma.2018.12.048.

1505 Kuang, X.X., Luo, X., Jiao, J.J., Liang, S.H., Zhang, X.L., Li, H.L., Liu, J.G. Using stable isotopes of  
1506 surface water and groundwater to quantify moisture sources across the Yellow River source region.  
1507 *Hydrological Processes*. 33(13): 1835-1850, 2019. DOI: 10.1002/hyp.13441.

1508 Kumar, A., Sanyal, P., Agrawal, S. Spatial distribution of  $\delta^{18}\text{O}$  values in river water in the Ganga River  
1509 Basin: insight into the hydrological processes. *Journal of Hydrology*. 571: 225-234, 2019. DOI:  
1510 10.1016/j.jhydrol.2019.01.044.

1511 Lai, J.S., Zou, Y., Zhang, J.L., Peres-Neto, P.R. Generalizing hierarchical and variation partitioning in  
1512 multiple regression and canonical analyses using the rdacca.hp R package. *Methods in Ecology and*  
1513 *Evolution*. 13(4): 782-788, 2022. DOI: 10.1111/2041-210X.13800.

1514 Lamontagne, S., Kirby, J., Johnston, C. Groundwater-surface water connectivity in a chain of ponds  
1515 semiarid river. *Hydrological Processes*. 35(4): e14129, 2021. DOI: 10.1002/hyp.14129.

1516 Letz, O., Siebner, H., Avrahamov, N., Egozi, R., Eshel, G., Dahan, O. The impact of geomorphology on  
1517 groundwater recharge in a semi-arid mountainous area. *Journal of Hydrology*. 603: 127029, 2021. DOI:  
1518 10.1016/j.jhydrol.2021.127029.

删除了: <https://doi.org/>

删除了: <https://doi.org/>

1521 Li, H., Xiang, W., Si, B.C., Min, M., Miao, C.H., Jin, J.J. Quantifying recharge mechanisms in low-hilly  
1522 areas of a loess region: Implications for the quantity and quality of groundwater. *Journal of Hydrology*.  
1523 643: 131982, 2024a. DOI: 10.1016/j.jhydrol.2024.131982.

1524 [Li, M.Y., Xie, Y.Q., Dong, Y.H., Wang, L.H., Zhang, Z.Y. Review: Recent progress on groundwater  
1525 recharge research in arid and semiarid areas of China. \*Hydrogeology Journal\*, 32\(1\), 9-30, 2024b. DOI:  
1526 \[10.1007/s10040-023-02656-z.\]\(#\)](#)

1527 Li, H.X., Han, S.B., Wu, X., Wang, S., Liu, W.P., Ma, T., Zhang, M.N., Wei, Y.T., Yuan, F.Q., Yuan, L.,  
1528 Li, F.C., Wu, B., Wang, Y.S., Zhao, M.M., Yang, H.W., Wei, S.B. Distribution, characteristics and  
1529 influencing factors of fresh groundwater resources in the Loess Plateau, China. *China Geology*. 4(3):  
1530 209-526, 2021. DOI: 10.31035/cg2021057.

1531 Li, Y. S. Effects of forest on water circle on the Loess Plateau. *Journal of Natural Resources*. 16(05):  
1532 427-432, 2001. DOI: 111451567011-81/4190641.

1533 Li, Y.R., Shi, W.H., Aydin, A., Beroya-Eitner, M.A., Gao, G.H. Loess genesis and worldwide distribution.  
1534 *Earth-Science Reviews*. 201: 102947, 2020. DOI: [10.1016/j.earscirev.2019.102947.](#)

1535 Li, Z., Chen, X., Liu, W.Z., Si, B.C. Determination of groundwater recharge mechanism in the deep  
1536 loessial unsaturated zone by environmental tracers. *Science of The Total Environment*. 586: 827-835,  
1537 2017. DOI: [10.1016/j.scitotenv.2017.02.061.](#)

1538 Li, Z., Coles, A.E., Xiao, J. Groundwater and streamflow sources in China's Loess Plateau on catchment  
1539 scale. *Catena*. 181: 104075, 2019. DOI: [10.1016/j.catena.2019.104075.](#)

1540 Lian, H.S., Yen, H., Yu, K., Zou, J.Y., Liu, C.X. Groundwater pollution becomes new constraint after  
1541 watershed-scale water quality restoration. *Journal of Hydrology*. 661: 133558, 2025. DOI:  
1542 [10.1016/j.jhydrol.2025.133558.](#)

1543 Liang, W., Bai, D., Wang, F.Y., Fu, B.J., Yan, J.P., Wang, S., Yang T.Y., Long, D., Feng, M.Q. Quantifying  
1544 the impacts of climate change and ecological restoration on streamflow changes based on a Budyko  
1545 hydrological model in China's Loess Plateau. *Water Resources Research*. 51: 6500-6519, 2015. DOI:  
1546 10.1002/2014WR016589.

1547 Liang, X.J. *Applied hydrogeology*. Beijing: Science Press, 2016.

1548 Liu, D.S. *Loess and the environment*. Science Press, Beijing, 1985.

1549 Liu, X., Song, X.F., Zhang, Y.H., Xia, J., Zhang, X.C., Yu, J.J., Long, D., Li, F.D., Zhang, B. Spatio-  
1550 temporal variations of  $\delta^2\text{H}$  and  $\delta^{18}\text{O}$  in precipitation and shallow groundwater in the Hilly Loess Region

删除了: <https://doi.org/>

删除了: <https://doi.org/>

删除了: <https://doi.org/>

删除了: <https://doi.org/>

1555 of the Loess Plateau, China. Environmental Earth Sciences. 63(5): 1105-1118, 2011. DOI:  
1556 10.1007/s12665-010-0785-y.

1557 Liu, Y.S., Chen, Z., Li, Y., Feng, W., Cao, Z. The planting technology and industrial development  
1558 prospects of forage rape in the loess hilly area: A case study of newly-increased cultivated land through  
1559 gully land consolidation in Yan'an, Shaanxi Province. Journal of Natural Resources. 32: 2065-2074, 2017.  
1560 DOI: 10.11849/zrzyxb.20161142.

1561 Liu, Y.S., Li, Y. Engineering philosophy and design scheme of gully land consolidation in Loess Plateau.  
1562 Transactions of the Chinese Society of Agricultural Engineering. 33(10): 1-9, 2017. DOI:  
1563 [10.11975/j.issn.1002-6819.2017.10.001](https://doi.org/10.11975/j.issn.1002-6819.2017.10.001)

1564 [Liu, Y.Z. Source analysis of precipitation chemical components on the Loess Plateau based on hydrogen](#)  
1565 [and oxygen stable isotopes\[D\]. Northwest A&F University, 2024.](#)  
1566 [DOI:10.27409/d.cnki.gxbnu.2024.001528.](https://doi.org/10.27409/d.cnki.gxbnu.2024.001528)

1567 Lu, Y.W. Study on typical hydrological characteristics of the vadose zone and spatiotemporal evolution  
1568 of potential groundwater recharge in the Chinese Loess Plateau. Yangling: Northwest A & F University,  
1569 2020. DOI: 10.11975/j.issn.1002-6819.2017.10.001.

1570 Lupi, L., Bertrand, L., Monferrán, M. V., Amé, M. V., del Pilar Diaz, M. Multilevel and structural  
1571 equation modeling approach to identify spatiotemporal patterns and source characterization of metals  
1572 and metalloids in surface water and sediment of the Ctlamochita River in Pampa region, Argentina.  
1573 Journal of Hydrology. 572: 403-413, 2019. DOI: 10.1016/j.jhydrol.2019.03.019.

1574 Manna, F., Murray, S., Abbey, D., Martin, P., Cherry, J., Parker, B. Spatial and temporal variability of  
1575 groundwater recharge in a sandstone aquifer in a semi-arid region. Hydrology and Earth System Sciences  
1576 Discussions. 2018: 1-36, 2018. DOI: 10.5194/hess-23-2187-2019.

1577 Medici, G., Munn, J. D., Parker, B. L. Delineating aquitard characteristics within a Silurian dolostone  
1578 aquifer using high-density hydraulic head and fracture datasets. Hydrogeology Journal. 32(6): 1663-1691,  
1579 2024. DOI: [10.1007/s10040-024-02824-9](https://doi.org/10.1007/s10040-024-02824-9).

1580 Meles, M.B., Bradford, S., Casillas-Trasvina, A., Chen, L., Osterman, G., Hatch, T., Ajami, H., Crompton,  
1581 O., Levers, L., Kisekka, I. Uncovering the gaps in managed aquifer recharge for sustainable groundwater  
1582 management: A focus on hillslopes and mountains. Journal of Hydrology. 639: 131615, 2024. DOI:  
1583 10.1016/j.jhydrol.2024.131615.

1584 Nachabe, M.H. Analytical expressions for transient specific yield and shallow water table drainage.

删除了:-

删除了: <https://doi.org/>

删除了: <https://doi.org/>

删除了: <https://doi.org/>

1589 Water Resources Research. 38 (10): 11-17, 2002. DOI: 10.1029/2001WR001071.

1590 Nicholson, S. E. Dryland Climatology. Cambridge University Press, 2011.

1591 Obuobie, E., Diekkruieger, B., Agyekum, W., Agodzo, S. Groundwater level monitoring and recharge  
1592 estimation in the White Volta River basin of Ghana. Journal of African Earth Sciences. 71-72: 80-86,  
1593 2012. DOI: 10.1016/j.jafrearsci.2012.06.005.

1594 Ouali, A.E., Roubil, A., Lahrach, A., Hmaidi, A.E., Ouali, A.E., Ousmana, H., Bouchaou, L. Assessments  
1595 of groundwater recharge process and residence time using hydrochemical and isotopic tracers under arid  
1596 climate: Insights from Errachidia basin (Central-East Morocco). Groundwater for Sustainable  
1597 Development. 25: 101145, 2024. DOI: 10.1016/j.gsd.2024.101145.

1598 Owuor, S. O., Butterbach-Bahl, K., Guzha, A. C., Rufino, M. C., Pelster, D. E., Díaz-Pinés, E., Breuer,  
1599 L. Groundwater recharge rates and surface runoff response to land use and land cover changes in semi-  
1600 arid environments. Ecological Processes, 5: 1-21, 2016. DOI: 10.1186/s13717-016-0060-6.

1601 Pe'csi, M. Loess is not just the accumulation of dust. Qaut Int. 7(8):1-21, 1990. DOI:10.1016/1040-  
1602 6182(90)90034-2.

1603 Qiao, J.B., Zhu, Y.J., Jia, X.X., Huang, L.M., Shao, M.A. Spatial variability of soil water for the entire  
1604 profile in the critical zone of the Loess Plateau. Advances in Water Science. 28(04): 515-522, 2017. DOI:  
1605 10.14042/j.cnki.32.1309.2017.04.005.

1606 Qu, S., Zhao, Y.Z., Li, M.H., Ren, X.H., Wang, C.Y., Yang, X., Hao, Y.L., Dong, S.G., Yu, R.H. Unveiling  
1607 sources and fate of sulfate in lake-groundwater system combined Bayesian isotope mixing model with  
1608 radon mass balance model. Water Research. 282: 123648, 2025. DOI: 10.1016/j.watres.2025.123648.

1609 Salek, M., Levison, J., Parker, B., Gharabaghi, B. CAD-DRASTIC: chloride application density  
1610 combined with DRASTIC for assessing groundwater vulnerability to road salt application. Hydrogeology  
1611 Journal. 26: 2379-2393, 2018. DOI: 10.1007/s10040-018-1801-7.

1612 Scanlon, B.R., Healy, R.W., Cook, P.G. Choosing appropriate techniques for quantifying groundwater  
1613 recharge. Hydrogeology Journal. 10(1): 18-39, 2022. DOI: 10.1007/s10040-001-0176-2.

1614 Shah, N., Ross, M. Variability in specific yield under shallow water table conditions. Journal of  
1615 Hydrologic Engineering. 14(12): 1290-1298, 2009. DOI: 10.1061/(ASCE)HE.1943-5584.0000121.

1616 Shi, H., Shao, M.A. Soil and water loss from the Loess Plateau in China. Journal of arid environments.  
1617 45(1): 9-20, 2000. DOI: 10.1006/jare.1999.0618.

1618 Tan, H.B., Liu, Z.H., Rao, W.B., Jin, B., Zhang, Y.D. Understanding recharge in soil-groundwater

删除了:.

删除了: <https://doi.org/>

删除了: 2020

删除了: <https://doi.org/>

删除了: Shi, P.J., Huang, Y.N., Yang, K.Y., Li, Z. Quantitative estimation of groundwater recharge in the thick loess deposits using multiple environmental tracers and methods. Journal of Hydrology. 603(8): 126895, 2021. DOI: <https://doi.org/10.1016/j.jhydrol.2021.126895>.

1628 systems in high loess hills on the Loess Plateau using isotopic data. *Catena*. 156: 18-29, 2017. DOI:  
1629 [10.1016/j.catena.2017.03.022](https://doi.org/10.1016/j.catena.2017.03.022).

1630 Tan, H.B., Wen, X.W., Rao, W.B., Bradd, J., Huang, J.Z. Temporal variation of stable isotopes in a  
1631 precipitation-groundwater system: implications for determining the mechanism of groundwater recharge  
1632 in high mountain hills of the Loess Plateau, China. *Hydrological Processes*. 30(10): 1491-1505, 2016.  
1633 DOI:[10.1002/hyp.10729](https://doi.org/10.1002/hyp.10729).

1634 Tetzlaff, D., Seibert, J., McGuire, K.J., Laudon, H., Burns, D.A., Dunn, S.M., Soulsby, C. How does  
1635 landscape structure influence catchment transit time across different geomorphic provinces?  
1636 *Hydrological Processes*. 23: 945-953, 2009. DOI:[10.1002/hyp.7240](https://doi.org/10.1002/hyp.7240).

1637 Tooth, S. Arid geomorphology: Changing perspectives on timescales of change. *Progress in Physical*  
1638 *Geography*. 36(2): 262-284, 2012. DOI: 10.1177/0309133311417943.

1639 Vries, J.J.D., Simmers, I. Groundwater recharge: an overview of processes and challenges. *Hydrogeology*  
1640 *Journal*. 10(1): 5-17, 2002. DOI: 10.1007/s10040-001-0171-7.

1641 Wan, H., Liu, W.G. An isotope study ( $\delta^{18}\text{O}$  and  $\delta^2\text{H}$ ) of water movements on the Loess Plateau of China  
1642 in arid and semiarid climates. *Ecological Engineering*. 8(93): 226-233, 2016. DOI:  
1643 [10.1016/j.ecoleng.2016.05.039](https://doi.org/10.1016/j.ecoleng.2016.05.039)

1644 Wang, L., Shao, M., Wang, Q.J., Gale, J. Historical changes in the environment of the Chinese Loess  
1645 Plateau. *Environmental Science & Policy*. 9: 675-684, 2006. DOI:[10.1016/j.envsci.2006.08.003](https://doi.org/10.1016/j.envsci.2006.08.003).

1646 Wang, W.Z., Sun, J.N., Xia, Y., Li, Z. Identifying hydraulic connectivity among the vadose zone,  
1647 unconfined and confined aquifers in the thick loess deposits using multiple tracers. *Journal of Hydrology*.  
1648 626: 130339, 2023. DOI:[10.1016/j.jhydrol.2023.130339](https://doi.org/10.1016/j.jhydrol.2023.130339).

1649 Wang, W.Z., Xia, Y., Sun, J.N., Liu, Y.Z., Li, P.Y., Han, F.P., Li, Z. Uncertainties in physical and tracer  
1650 methods in actual groundwater recharge estimation in the thick loess deposits of China. *Journal of*  
1651 *Hydrology*. 634: 131127, 2024. DOI:[10.1016/j.jhydrol.2024.131127](https://doi.org/10.1016/j.jhydrol.2024.131127).

1652 Wang, Y.Q., Shao, M.A., Sun, H., Fu, Z.H., Fan, J., Hu, W., Fang, L.C. Response of deep soil drought to  
1653 precipitation, land use and topography across a semiarid watershed. *Agricultural and Forest Meteorology*.  
1654 282-283: 107866, 2020. DOI:[10.1016/j.agrformet.2019.107866](https://doi.org/10.1016/j.agrformet.2019.107866).

1655 Wu, M.L. *The structural equation model: AMOS operation and application*. Chongqing: Chongqing  
1656 University Press, 2010.

1657 Xiang W. Study on soil evaporation and groundwater recharge based on stable isotopes in the Loess

删除了: <https://doi.org/>

删除了: <https://doi.org/>

删除了: <https://doi.org/>

删除了: <https://doi.org/>

删除了: <https://doi.org/>

删除了: <https://doi.org/>

删除了: <https://doi.org/>

删除了: <https://doi.org/>

删除了: Wang, Y.Q., Sun, H., Zhao, Y.L. Characterizing spatial-temporal patterns and abrupt changes in deep soil moisture across an intensively managed watershed. *Geoderma*. 341: 181-194, 2019. DOI: <https://doi.org/10.1016/j.geoderma.2019.01.044>.

1671 Plateau at regional scale. Yangling: Northwest A & F University, 2020. DOI:  
1672 10.27409/d.cnki.gxbnu.2021.000025.

1673 [Xiang, W., Si, B.C., Biswas, A., Li, Z. Quantifying dual recharge mechanisms in deep unsaturated zone](#)  
1674 [of Chinese Loess Plateau using stable isotopes. Geoderma. 337: 773-781, 2019. DOI:](#)  
1675 [10.1016/j.geoderma.2018.10.006.](#)

1676 Xie, T.T., Zhao, H.J., Chen, G.K., Lin, H.H. Land Use Patterns and River Nitrate Dynamics in Karst  
1677 Regions: Insights from High-Resolution Sentinel-2 Imagery and Partial Least Squares Structural  
1678 Equation Modeling Analysis. Environmental Engineering Science, 2025. DOI:10.1089/ees.2024.0272.

1679 Xu, P., Weng, B.S., Gong, X.Y., Xia, K.B., Yan, D.H., Wang, H. Estimation of shallow groundwater  
1680 recharge in central Qinghai-Tibet Plateau by combining unsaturated zone simulation and improved water  
1681 table fluctuation method. Journal of Hydrology. 630: 130689, 2024. DOI:10.1016/j.jhydrol.2024.130689.

1682 Xu, Y., Beekman, H. E. Review: Groundwater recharge estimation in arid and semi-arid southern Africa.  
1683 Hydrogeology Journal. 27(3): 929-943, 2019. DOI: 10.1007/s10040-018-1898-8.

1684 Xu, Z.Y., Zhao, Y.J., Chen, J.J. Research of fractural efficacy on mechanisms governing water flow in  
1685 unsaturated loess. Journal of Changchun University of Earth Sciences. 23(03): 326-329, 1993.

1686 Xue, S.B., Li, P., Cui, Z.W., Li, Z.B. The influence of different check dam configurations on the  
1687 downstream river topography and water-sediment relationship. Journal of Hydrology. 656: 133046, 2025.  
1688 DOI: 10.1016/j.jhydrol.2025.133046.

1689 [Yang, N., Wang, G.C. Spatial variation of water stable isotopes of multiple rivers in southeastern Qaidam](#)  
1690 [Basin, northeast Qinghai-Tibetan Plateau: Insights into hydrologic cycle. Journal of Hydrology. 628:](#)  
1691 [130464, 2023. DOI: 10.1016/j.jhydrol.2023.130464.](#)

1692 [Yu L.L., Ji, Z.X., Wang, L. Characteristics of Perched Water Recharge in the Dam Land of Yangjuangou](#)  
1693 [Small Watershed on the Loess Plateau. Acta Pedologica Sinica. 62\(4\): 983-997, 2025. DOI :](#)  
1694 [10.11766/trxb202404290178.](#)

1695 [Yu, Y.L., Jin, Z., Chu, G.C., Zhang, J., Wang, Y.Q., Zhao, Y.L. Effects of valley reshaping and](#)  
1696 [damming on surface and groundwater nitrate on the Chinese Loess Plateau. Journal of Hydrology.](#)  
1697 [584: 124702, 2020.](#)

1698 [Zhang, H., Xu, Y.X., Kanyerere, T. A review of the managed aquifer recharge: Historical development,](#)  
1699 [current situation and perspectives. Physics and Chemistry of the Earth, Parts A/B/C. 118-119: 102887,](#)  
1700 [2020. DOI: 10.1016/j.pce.2020.102887.](#)

删除了:

删除了: <https://doi.org/>

删除了: <https://doi.org/>

删除了: Yan, T.B., Wang, D.Q. The Recharge Mechanism of Unconfined Groundwater in the Loess of the Luochuan Yuan and Its Water Bearing Characteristics. Geological Review. 5(29): 418-427, 1983. DOI: 10.16509/j.georeview.1983.05.003

删除了: <https://doi.org/>

删除了: Yang, X.P., Liu, T., Yuan, B.Y. The Loess Plateau of China: Aeolian sedimentation and fluvial erosion, both with superlative rates. Geomorphological Landscapes of the World. 1: 275-282, 2009. DOI: 10.1007/978-90-481-3055-9\_28.

设置了格式: 字体: 五号

删除了: Yuan, S., Li, Z., Chen, L., Li, P., Zhang, Z., Zhang, J., Wang, A. Effects of a check dam system on the runoff generation and concentration processes of a catchment on the Loess Plateau. International Soil and Water Conservation Research. 10(1): 86-98, 2022. <https://doi.org/DOI:10.1016/j.iswcr.2021.06.007>.

1721 Zhang, J., Chen, H.S., Fu, Z.Y., Wang, F., Wang, K.L. Towards hydrological connectivity in the karst  
 1722 hillslope critical zone: Insight from using water isotope signals. *Journal of Hydrology*. 617: 128926, 2022.  
 1723 DOI: 10.1016/j.jhydrol.2022.128926.

1724 Zhang, Y.H., Wu, Y.P. Oxygen and Hydrogen Isotopes in Precipitation in Heihe River Basin, China.  
 1725 *Journal of Glaciology and Geocryology*. 31(1): 34-39, 2009. DOI: 100020240(2009)0120034206.

1726 [Zhao, Y., Wang, L. Determination of groundwater recharge processes and evaluation of the “two water](#)  
 1727 [worlds” hypothesis at a check dam on the Loess Plateau. \*Journal of Hydrology\*. 595: 125989, 2021. DOI:](#)  
 1728 [10.1016/j.jhydrol.2021.125989.](#)

1729 Zhao, Y.L., Wang, Y.Q., Sun, H., Lin, H., Jin, Z., He, M.N., Yu, Y.L., Zhou, W.J., and An, Z. S. Intensive  
 1730 land restoration profoundly alters the spatial and seasonal patterns of deep soil water storage at watershed  
 1731 scales. *Agriculture, Ecosystems & Environment*. 280: 129-141, 2019. DOI: 10.1016/j.agee.2019.04.028.

1732 [Zhao, Y.L., Wang, Y.Q., Zhou, J.X., Qi, L.J., Zhang, P.P. Spatiotemporal variation and controlling factors](#)  
 1733 [of dried soil layers in a semi-humid catchment and relevant land use management implications. \*CATENA\*.](#)  
 1734 [240: 107973, 2024. DOI: 10.1016/j.catena.2024.107973.](#)

1735 Zhu, Y.J., Jia, X.X., Shao, M.A. Loess thickness variations across the loess plateau of China. *Surveys in*  
 1736 *Geophysics*. 39(4): 715-727, 2018. DOI: 10.1007/s10712-018-9462-6.

删除了: <https://doi.org/>

删除了: Zhao, Y., Wang, L. Determination of groundwater recharge processes and evaluation of the ‘two water worlds’ hypothesis at a check dam on the Loess Plateau. *Journal of Hydrology*. 595: 125989, 2021. <https://doi.org/10.1016/j.jhydrol.2021.125989>.

删除了: Zhao, Y.L., Wang, Y.Q., Hu, W., Sun, H., Qi, L.J., Xu, L., Song, Y., Zhang, P.P. Intensive land restoration projects alter mechanisms underpinning spatiotemporal soil moisture variability at a catchment scale: A case study in China. *Journal of Hydrology*. 630: 130739, 2024. [https://doi.org/DOI: 10.1016/j.jhydrol.2024.130739](https://doi.org/DOI:10.1016/j.jhydrol.2024.130739).

删除了: <https://doi.org/>

删除了: <https://doi.org/>

1751 **Appendix A**

1752 1. The specific yield of different soil textures is shown.

1753 Table A1. The specific yield of different texture of soil (adapted from Liang, 2016)

Texture	Average Specific Yield	Minimum Specific Yield	Maximum Specific Yield	Coefficient of Variation (%)
Clay	0.02	0.00	0.05	59
Silt	0.08	0.03	0.19	60
Sandy Clay	0.07	0.03	0.12	44
Fine Sand	0.21	0.10	0.28	32
Medium Sand	0.26	0.15	0.32	18
Coarse Sand	0.27	0.20	0.35	18
Gravelly Sand	0.25	0.20	0.35	21
Fine Gravel	0.25	0.21	0.35	18
Medium Gravel	0.23	0.13	0.26	14
Coarse Gravel	0.22	0.12	0.26	20

1754

1755 2. The isotopic composition ( $\delta^2\text{H}$  and  $\delta^{18}\text{O}$ ) of various water sources in the rainy and dry seasons is shown.

1756 Table A2. Isotopic composition ( $\delta^2\text{H}$  and  $\delta^{18}\text{O}$ ) of various water sources in the rainy and dry seasons

	Rainy season		Dry season	
	$\delta^2\text{H}$	$\delta^{18}\text{O}$	$\delta^2\text{H}$	$\delta^{18}\text{O}$
Rainfall	$-36.6 \pm 20.4\text{‰}$	$-5.6 \pm 2.3\text{‰}$	$-31.0 \pm 23.2\text{‰}$	$-4.9 \pm 3.0\text{‰}$
Pond water	$-40.5 \pm 13.1\text{‰}$	$-4.1 \pm 2.3\text{‰}$	$-24.5 \pm 6.9\text{‰}$	$-0.8 \pm 1.3\text{‰}$
Spring water	$-67.3 \pm 2.6\text{‰}$	$-9.0 \pm 0.4\text{‰}$	$-68.4 \pm 2.2\text{‰}$	$-9.0 \pm 0.4\text{‰}$
Pore water	$-66.3 \pm 3.1\text{‰}$	$-9.0 \pm 0.6\text{‰}$	$-65.4 \pm 3.8\text{‰}$	$-8.5 \pm 0.6\text{‰}$
Fissure water	$-65.0 \pm 3.8\text{‰}$	$-8.8 \pm 0.9\text{‰}$	$-64.5 \pm 5.5\text{‰}$	$-8.5 \pm 0.9\text{‰}$

1757

删除了: 1. The typical loess landforms on the Loess Plateau is shown.

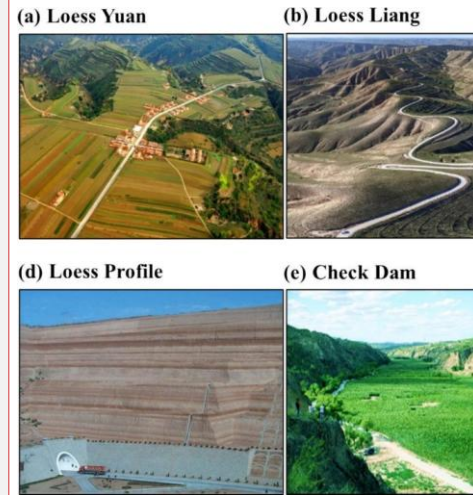


Fig. A1. Typical loess landforms are (a) Loess Yuan, (b) Loess Liang, and (c) Loess Mao. (d) A loess profile, (e) check dams and (f) terraces on the Chinese Loess Plateau. (adapted from Jia et al., 2024)

2

删除了: 3

删除了: 4. The chloride concentrations of various water sources in the rainy and dry seasons is shown.

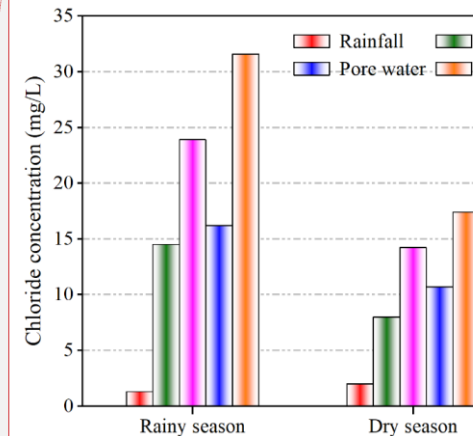


Fig. A2. Chloride concentrations of various water sources in the rainy and dry seasons.